Convergence analysis of linear or quadratic X-FEM for curved free boundaries

Guilhem Ferté, Patrick Massin, Nicolas Moes

Convergence analysis of linear or quadratic X-FEM for curved free boundaries

G. Ferté[a,b,*], P. Massin[a], N. Moës[b]

[a] *LaMSid, UMR EDF – CNRS – CEA, UMR 8193, EDF R&D, 1 av. du général de Gaulle, 92141 Clamart, France*
[b] *GeM UMR Ecole Centrale de Nantes – Université de Nantes – CNRS, Ecole Centrale de Nantes, 1 rue de la Noë, BP 92101, 44321 Nantes, France*

The aim of this paper is to provide a-priori error estimates for problems involving curved interfaces and solved with the linear or quadratic extended finite-element method (X-FEM), with particular emphasis on the influence of the geometry representation and the quadrature. We focus on strong discontinuity problems, which covers the case of holes in a material or cracks not subjected to contact as the main applications. The well-known approximation of the curved geometry based on the interpolated level-set function and straight linear or curved quadratic subcells is used, whose accuracy is quantified by means of an appropriate error measure. A priori error estimates are then derived, which depend upon the interpolation order of the displacement, and foremost upon the above error measure and the quadrature scheme in the subcells. The theoretical predictions are successfully compared with numerical experiments.

Keywords: Higher-order X-FEM; A-priori error estimates; Curved boundaries; Quadrature scheme

1. Introduction

The extended finite element method (X-FEM) is an extension to the classical finite element method introduced by Moës, Dolbow and Belytschko in [1] which allows easy handling of problems with jumps or singularities. Adequate

* Corresponding author at: LaMSid, UMR EDF – CNRS – CEA, UMR 8193, EDF R&D, 1 av. du général de Gaulle, 92141 Clamart, France. Tel.: +33 147655611.
E-mail addresses: guilhem.ferte@edf.fr, guilhemferte@hotmail.com (G. Ferté), patrick.massin@edf.fr (P. Massin), nicolas.moes@ec-nantes.fr (N. Moës).

resolution of such problems usually widely relies on the quality of the mesh, which should conform to the interface geometry. In particular, problems with evolving interfaces should be addressed with elaborated remeshing tools (see [2–4]). The X-FEM circumvents the difficulty by a local enrichment of the polynomial interpolation space with non-polynomial functions, based on the partition of unity method [5]. This enables a full independence of the mesh with respect to the interface location.

The extension of the X-FEM to higher order elements was first considered by Stazi, Belytschko et al. in [6] with the aim of describing cracks. Relying on the work of Chessa [7] on the partition of unity, they proposed a quadratic interpolation for the classical part of the displacement but a linear one for the enriched Heaviside and crack-tip part. Shortly after, Zi and Belytschko [8] considered the use of higher-order elements to describe cohesive cracks. To this purpose, they removed crack-tip enrichments but used a corrected Heaviside enrichment instead at the cohesive tip to account for discontinuities ending at the interior of an element. This absence of crack tip enrichment allowed the authors to use quadratic interpolation for the enriched Heaviside part as well (see [8]). Later on, Laborde and coworkers [9] extensively discussed crack-tip enrichment strategies that can be used with higher-order interpolation for the Heaviside enrichment. Despite the singularity, they recover the optimal convergence by enriching with the crack-tip functions on a fixed area. As this makes the conditioning number to soar, they proposed corrections with degree-of-freedom gathering (the rate of convergence being suboptimal, short of a 0.5 exponent) and pointwise matching (optimal). Alternative strategies were also proposed to restore acceptable conditioning without damaging the convergence, by means of enrichment with cutoff functions [10], vectorial enrichments [11] or both combined [12], or enrichment over a fixed area with an appropriate preconditioner [13]. This paper is restricted to Heaviside enrichment, but the above bibliography highlights existing tools to extend it to crack-tips while preserving both optimal convergence and acceptable conditioning.

In early papers about higher-order X-FEM, the authors highlighted the opportunity to better describe crack curvature. Stazi and Belytschko [6] interpolated the level set function using the same quadratic shape functions as those of the displacement. Based on the isozero of this interpolant, they would construct a quadrature scheme based on a linear subdivision. Later on, Legay, Wang and Belytschko [14] would again consider the isozero of the level-set functions, but use quadratic curved subcells for the quadrature. The authors observed suboptimal rates for curved interfaces and optimal rates for straight ones, suggesting that a poor representation of the geometry would hinder the convergence. More recently, and almost simultaneously, Cheng and Fries in [15], Dréau et al. in [16,17], Moumnassi and coworkers [18] also stressed out experimentally suboptimal rates for higher-order formulations when used along with a linear description of the geometry, provided the same grid is used as a starting point for the quadrature and the bulk fields. All three papers proposed successful remedies to the problems, namely:

1. the description of the crack geometry on a finer subgrid, in [16–18], so that piecewise-linear cuts over relatively small subcells drops the quadrature error to be as small as the interpolation error,
2. curved subcells with one curved 4-node edge in [15].

Despite these experiments, to our knowledge the link between the description of the geometry on the one hand, the quadrature rule in the subcells on the other and the error of the problem was never theoretically quantified to a predictive rule with X-FEM. This is the task that we propose to examine in this paper.

In this paper, the approach of Legay and coworkers [14] is adopted for the interface resolution: starting from the interpolated level set on the finite-element mesh, classical subdivision of cut elements into straight triangles or curved quadratic 6-node triangles is carried out. Each such subcell is then considered as belonging to one or the other side of the interface.

An error measure is provided in part 4 to assess the accuracy of this geometrical representation. Corresponding theoretical orders of convergence are provided and checked against numerical experiments. We link in part 5 geometrical representation, quadrature and convergence in X-FEM, based on the work of [19,20] in FEM. To this aim, we derive a priori estimates as functions of the above geometrical error measure, the quadrature scheme and the interpolation order of the displacement. In part 6, the estimates are validated by numerical experiments.

The main result of this article is that, in practice, it suffices to perform a subdivision after the same order than the interpolation and use the related typical quadrature scheme to get optimality. However, the theory allows to find out problematic cases that have to be handled with thorough consideration.

2. Formulation of the continuous problem

We consider an elastic body occupying a domain Ω in $\mathbb{R}^2$, which is mathematically a bounded open set. This body is cut through by a curved interface Γ, which can typically be a crack or a hole. In this way, Ω is separated into two open sets $\Omega_i,\ i \in \{1,2\}$, so that $\Omega = \Omega_1 \cup \Omega_2 \cup \Gamma$. The restriction of any field $\boldsymbol{v}$ to Ω_i is denoted by $\boldsymbol{v}_i$. For each body, the remaining of the boundary $\partial\Omega_i \setminus \Gamma$ is composed of non-overlapping parts Γ_u^i and Γ_g^i where conditions are prescribed on the displacement $\boldsymbol{u}_i$ and the surface force distribution $\boldsymbol{g}_i$, respectively. We assume that Γ_u^i has nonzero measure. Interface Γ is assumed to be traction free, which means that both parts constitute non-interacting solids. Holes in a material and cracks are the main applications of this case of study.

The body is subjected to volume forces $\boldsymbol{f}_i$ in addition to the surface loads. Small displacements and strains are assumed. The equations in Ω_i read:

$$\nabla \cdot \boldsymbol{\sigma}_i + \boldsymbol{f}_i = 0 \quad \text{in } \Omega_i \tag{1}$$

$$\boldsymbol{\sigma}_i \cdot \boldsymbol{n}_i = \boldsymbol{g}_i \quad \text{on } \Gamma_g^i \tag{2}$$

$$\boldsymbol{u}_i = 0 \quad \text{on } \Gamma_u^i \tag{3}$$

$$\boldsymbol{\sigma}_i \cdot \boldsymbol{n}_i = \boldsymbol{0} \quad \text{on } \Gamma \tag{4}$$

where $\boldsymbol{\sigma}_i$ is the Cauchy stress tensor, defined from the elasticity fourth-order tensor $\boldsymbol{A}_i$ and the strain tensor $\boldsymbol{\epsilon}_i = \frac{1}{2}\left(\nabla \boldsymbol{u}_i + \nabla \boldsymbol{u}_i^{\mathrm{T}}\right)$, as $\boldsymbol{\sigma}_i = \boldsymbol{A}_i \cdot \boldsymbol{\epsilon}_i$.

In what follows, we adopt classical notations for the functional spaces: $W^{m,p}(\Omega)$ denotes the Sobolev space of functions v for which all derivatives up to order m lie in $L^p(\Omega)$. In other words, for any multi-index $\alpha := (\alpha_1, \alpha_2)$ whose size $|\alpha| = \alpha_1 + \alpha_2$ is less than m, it holds $\partial^\alpha v := \frac{\partial^{|\alpha|} v}{\partial x_1^{\alpha_1} \partial x_2^{\alpha_2}} \in L^p(\Omega)$. The associated semi-norm is denoted $|\cdot|_{m,p,\Omega}$, and the associated norm $\|\cdot\|_{m,p,\Omega}$. Classically, index p is omitted when it is 2 so that we note $H^m(\Omega) := W^{m,2}(\Omega)$ and $\|v\|_{m,\Omega} := \|v\|_{m,2,\Omega}$. We also introduce product spaces $H^m(\Omega_1) \times H^m(\Omega_2)$, which are endowed with the broken norm $\|v\|^2_{m,\Omega_1\cup\Omega_2} := \|v\|^2_{m,\Omega_1} + \|v\|^2_{m,\Omega_2}$. In this paper, C will denote a generic non-negative constant, and c a strictly positive constant.

The components of the solution belong to $V := \{v \in H^1(\Omega_1) \times H^1(\Omega_2),\ v|_{\Gamma_u^i} = 0,\ i \in \{1,2\}\}$. A bilinear form $a \in \mathcal{L}(V^2 \times V^2; \mathbb{R})$ and linear form $b \in \mathcal{L}(V^2; \mathbb{R})$ are defined as:

$$\text{For } (\boldsymbol{u}, \boldsymbol{v}) \in V^2 \times V^2, \quad a(\boldsymbol{u}, \boldsymbol{v}) := \sum_{i=1}^{2} \int_{\Omega_i} \boldsymbol{\sigma}_i(\boldsymbol{u}_i) : \boldsymbol{\epsilon}_i(\boldsymbol{v}_i) dx \tag{5}$$

$$\text{For } \boldsymbol{v} \in V^2, \quad l(\boldsymbol{v}) := \sum_{i=1}^{2} \int_{\Omega_i} \boldsymbol{f}_i \cdot \boldsymbol{v}_i dx + \int_{\Gamma_g^i} \boldsymbol{g}_i \cdot \boldsymbol{v}_i ds. \tag{6}$$

The resulting weak formulation consists in finding $\boldsymbol{u} \in V^2$, such that $\forall \boldsymbol{v} \in V^2$:

$$a(\boldsymbol{u}, \boldsymbol{v}) = l(\boldsymbol{v}). \tag{7}$$

Eq. (7) constitutes a vectorial second-order problem. For the sake of conciseness, and as is very common in finite-element analysis, we shall in the mathematical developments of this paper rather work with a scalar second-order elliptic problem: this corresponds to a heat diffusion problem through a cracked structure. All theorems of this paper are given in the scalar setting, but their vectorized counterparts could be derived in a similar way. We set $a \in \mathcal{L}(V \times V; \mathbb{R})$ as:

$$a(u, v) := \sum_{i=1}^{2} \int_{\Omega_i} \nabla u_i \cdot \boldsymbol{A}_i \cdot \nabla v_i dx. \tag{8}$$

Here is $\boldsymbol{A}_i$ the conductivity second-order tensor, whose components are assumed to have regularity properties except across the interface: for $i \in \{1,2\}$ and $(k,l) \in \{1,2\}^2$, $(\boldsymbol{A}_i)_{kl} \in L^\infty(\Omega_i)$. This obviously ensures the continuity of a. Tensor $\boldsymbol{A}_i$ is also supposed to verify an ellipticity property, that is to say there exists $c > 0, \forall i \in \{1,2\}$,

$\forall \boldsymbol{x} \in \Omega_i, \forall \boldsymbol{\xi} \in \mathbb{R}^2, \left|\boldsymbol{\xi}^T \cdot \boldsymbol{A}_i(\boldsymbol{x}) \cdot \boldsymbol{\xi}\right| \geq c|\boldsymbol{\xi}|^2$. This makes a coercive. The source terms are $f_i \in L^2(\Omega_i)$ and we introduce $l \in \mathcal{L}(V; \mathbb{R})$ as:

$$l(v) := \sum_{i=1}^{2} \int_{\Omega_i} f_i v_i dx. \tag{9}$$

Again, the problem may be written as (7).

3. The discrete problem

3.1. The approximation of the geometry

Since the X-FEM is widely used to describe propagating interfaces, the interface is usually implicitly represented, by means of a signed distance function on Ω, called the level-set function (see e.g. [21]).

Assumption (H0). The existence of a level-set function ϕ is assumed in a 2δ-fixed-width strip S_δ centered on the interface, whose isozero coincides with the interface:

$$\Gamma = \{\boldsymbol{x}, \phi(\boldsymbol{x}) = 0\}. \tag{10}$$

This assumption is fully discussed in Appendix A, where a rigorous definition is given under regularity assumptions on the interface, the semi-width δ being related to the minimal radius of curvature.

We suppose that the whole domain Ω is meshed with a family $\mathcal{T}_h$ of triangular affine meshes, regardless of the location of the interface. We now aim at building an approximated conforming subdivision within cut elements. The first stage consists in interpolating the level-set function, by:

$$\phi_h(\boldsymbol{x}) = \sum_{j \in \mathcal{N}_h} N_j(\boldsymbol{x}) \phi_j \tag{11}$$

where $\mathcal{N}_h$ denotes the nodes of the mesh, N_j the shape function of order g associated with node j, and ϕ_j the values of the exact level-set function at this node (see Fig. 1(a)). Exponent g is thus the representation order of the geometry. If $g = 1$, this amounts to the well-known linear subdivision.

The idea is then to rely in a second stage on the iso-zero curve Γ_ϕ of the interpolated level-set function (represented in Fig. 1(b)) to build an approximation of the interface. If $g = 1$, two intersection points are computed to determine the border of linear conforming subcells. If $g = 2$, an additional middle point is determined on Γ_ϕ, using the perpendicular bisector to the segment linking the previous points (see Fig. 1(c)). The cut element is then subdivided into quadratic triangular subcells (see Fig. 1(d)), an edge of which interpolates the three points on the isozero curve. This edge is finally the approximation Γ_h of the interface (see Fig. 1(d)): any subcell E then fully belongs to one or the other side of the interface. Approximated bodies Ω_i^h may then be identified as in Fig. 1(d).

About Γ_ϕ and Γ_h being different curves when $g = 2$.

When $g = 1$, Γ_ϕ is a line, and since two points determine a line, Γ_ϕ and Γ_h necessarily coincide. On the contrary, when $g = 2$, Γ_ϕ is a conic section (the 2D case of quadric surface), and as such is determined in a unique manner not by *three*, but by *five* points. Consequently, having three points in common does not ensure that the quadratic-subcell edge Γ_h coincides with Γ_ϕ: they might still be different conic sections.

3.2. The interpolation of the field of unknowns

Again, $\mathcal{T}_h$ denotes a family of affine triangular meshes of Ω. Since in the X-FEM the position of the interface is independent of the mesh, this does not prevent the representation of arbitrary curved interfaces. Family $\mathcal{T}_h$ is assumed to be quasi-uniform and regular, that is to say for $K \in \mathcal{T}_h$, denoting h_K the radius of the smallest circle containing K and ρ_K the radius of the largest circle included in K and setting the characteristic mesh size $h := \max_K h_K$, we have:

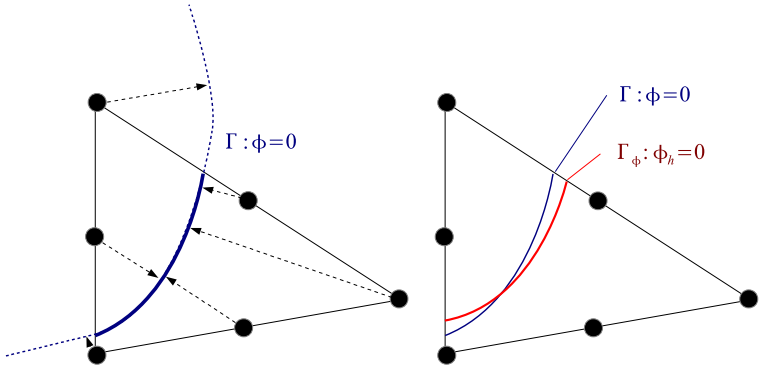

(a) Computation of nodal level sets.

(b) Quadratic interpolation from nodal values.

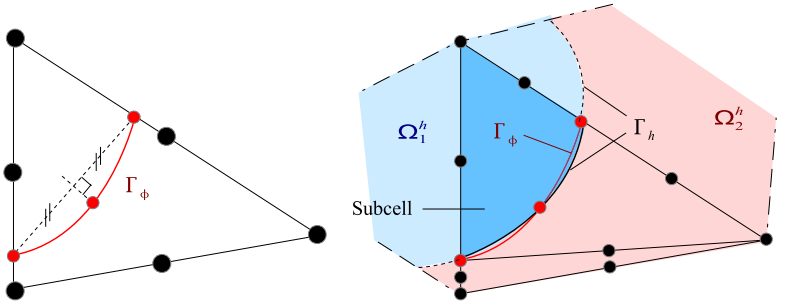

(c) Determination of some points on the interpolated level-set isozero.

(d) Subdivision with corresponding quadratic triangles and approximated domains.

Fig. 1. Subdivision of cut elements in the case where $g = 2$.

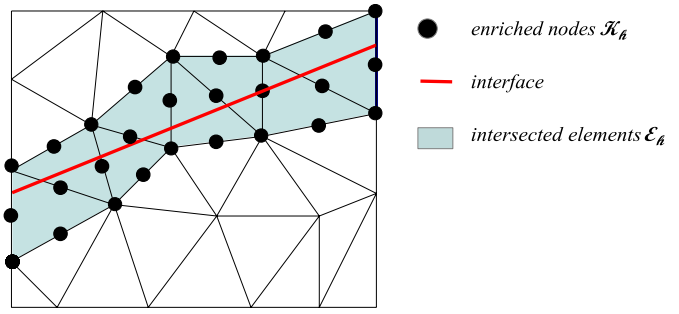

Fig. 2. Interface, mesh not matching the interface and enriched nodes, in the case $p = 2$.

Assumption (H1). There exists a constant C independent of h and K such that $\frac{h}{\rho_K} \leq C$. This ensures that the angles of triangle K are uniformly bounded away from zero.

In order to account for the field jump across the interface, the classical finite element approximation is enriched with a Heaviside-like function (see [1]):

$$V_h := \left\{ \sum_{i \in \mathcal{N}_h} a_i N_i(\boldsymbol{x}) + \sum_{j \in \mathcal{K}_h} b_j N_j(\boldsymbol{x}) H(\boldsymbol{x}), a_i \in \mathbb{R}, b_i \in \mathbb{R} \right\}. \tag{12}$$

In this expression N_i is the shape function of order p at node i, with $p \in \{1, 2\}$, $\mathcal{K}_h$ is the set of enriched nodes – the nodes whose shape function is not identically zero on the interface, as pictured in Fig. 2 – and H is the Heaviside-like

function used to represent the jump:

$$H(\boldsymbol{x}) = \begin{cases} -1 & \text{if } \boldsymbol{x} \in \Omega_1^h \\ +1 & \text{if } \boldsymbol{x} \in \Omega_2^h. \end{cases} \tag{13}$$

Note that the interpolation order p may be different from the representation order g of the geometry. We denote $\mathcal{E}_h$ the set of cut elements.

4. The accuracy of the geometry description

We shall now be equipped with an error measure for assessing the accuracy of the geometry description:

Definition 4.1. The interface resolution is introduced as $\epsilon := \max_{\boldsymbol{x}\in\Gamma} \left(\min_{\boldsymbol{x}'\in\Gamma_h} |\boldsymbol{x} - \boldsymbol{x}'|\right)$. Of course, ϵ depends upon h, but this dependence is omitted in the notation for the sake of conciseness. The dependence of ϵ upon h indicates a convergence in L^∞-norm.

This measure is an extension to X-FEM of Definition 3.1 in [22] for classical FEM. Geometrically, this means that for any subdivision, we have $\Gamma_h \subset S_\epsilon$, where S_ϵ is the 2ϵ-fixed-width strip centered on Γ: the interface is thus said to be ϵ-resolved by the subdivision.

4.1. Interpolating the level-set function

The first stage of our description consists in approximating the level-sets. For $K \in \mathcal{T}_h$, let $P_g(K)$ be the space of polynomials of total order g on K. Let I_g be the standard nodal interpolation operator. We have:

Lemma 4.1. *Let $g \in \{1, 2\}$, $\delta' < \delta$ and assume the level-set ϕ to satisfy $\phi \in C^{g+1}(S_\delta)$. Then for $h \leq h_0 := \delta - \delta'$ the interpolation estimate $\|\phi - I_g\phi\|_{0,\infty,S_{\delta'}} \leqslant Ch^{g+1}\|\phi\|_{g+1,\infty,S_\delta}$ holds.*

Proof. We apply [19, Theorem 3.1.6] (interpolation with affine meshes). Since $h \leq h_0 := \delta - \delta'$, ϕ is well-defined on all elements $K \in \mathcal{T}_h$ verifying $K \cap S_{\delta'} \neq \emptyset$. □

4.2. Constructing subcells

In order to analyze the error that we have made approximating Γ_ϕ by Γ_h (second stage), we should introduce, for the purpose of the demonstration exclusively, subcells which exactly resolve a curved interface (see [23]), referred to as transfinite subcells (see Fig. 3). Their mappings are no longer polynomial but simply analytical, and constructed by transfinite interpolation from the analytical expression of the curved edge to be matched. In order to evaluate the error mentioned above, we have constructed a mapping $\tilde{F}_{\tilde{E}}$ for transfinite subcells and compared it with the polynomial mapping F_E of classical ones. The analysis is detailed in Appendix B. Its main result reads as follows (Lemma B.1): under the assumption that Γ_ϕ admits a local C^{g+1}-parametrization $\boldsymbol{f}_\phi$ from a segment I, which is the case since Γ_ϕ is a conic-section, we have:

$$\|\tilde{F}_{\tilde{E}} - F_E\|_{g+1,\infty,\hat{K}} \leq Ch^{g+1}|\boldsymbol{f}_\phi|_{g+1,\infty,I}. \tag{14}$$

We are now in a position to give an estimate for the whole process:

Theorem 4.1. *Let $g \in \{1, 2\}$ be the representation order of the geometry. Assume interface Γ to have a geometric continuity G_{g+2}. Then the interface is $O(h^{g+1})$ resolved by the subdivision, that is to say $\epsilon \leq Ch^{g+1}$.*

Appendix A may be consulted for a comprehensive definition of geometric continuity.

Proof. Since Γ has a geometric continuity G_{g+2}, after Lemma A.1 we have $\phi \in C^{g+1}(S_\delta)$. We may therefore apply Lemma 4.1, which for $\boldsymbol{x} \in \Gamma_h$ gives (see Fig. 4):

$$\begin{aligned} |\phi(x)| &\leq \min_{x'\in\Gamma_\phi} \left(|\phi(\boldsymbol{x}') - \phi_h(\boldsymbol{x}')| + |\boldsymbol{x}' - \boldsymbol{x}|\right) \\ &\leq Ch^{g+1}|\phi|_{g+1,\infty,S_\delta} + \min_{x'\in\Gamma_\phi} \left(\|\boldsymbol{x}' - \boldsymbol{x}\|\right). \end{aligned} \tag{15}$$

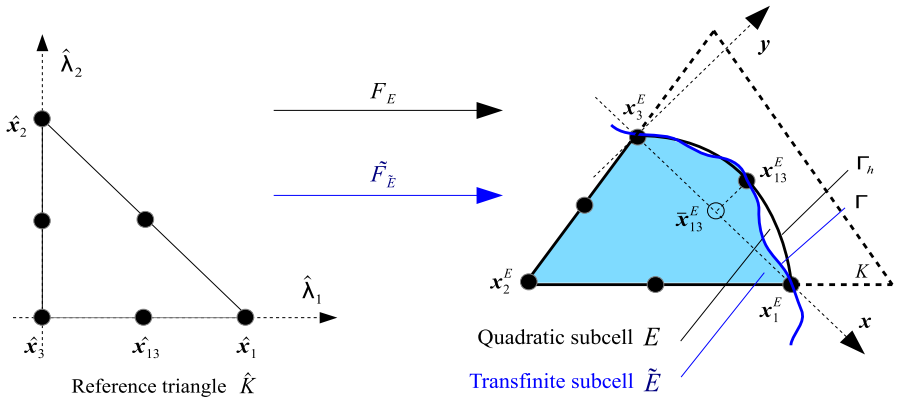

Fig. 3. Classical and transfinite subcells, in the case where $g = 2$.

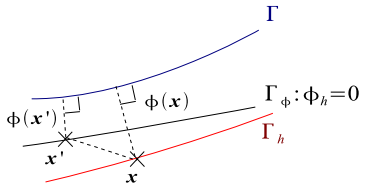

Fig. 4. Decomposition of the errors.

We may then apply Lemma B.1. to any subcell E with a curved edge for each cut parent element:

$$|\phi(\boldsymbol{x})| \leq Ch^{g+1} \left(|\phi|_{g+1,\infty,S_\delta} + |\boldsymbol{f}_\phi|_{g+1,\infty,I} \right). \tag{16}$$

Let $\begin{cases} I \to \mathbb{R} \\ s \to f_\phi(s) = (x(s), y(s)) \end{cases}$ be a parametrization of Γ_ϕ. Then we have $\forall s \in I$,

$$\boldsymbol{f}'_\phi(s) \cdot \nabla \phi_h(x(s), y(s)) = 0. \tag{17}$$

It may be deduced that parametrization $\boldsymbol{f}_\phi$ may be chosen such that $y'(s) = \frac{\partial \phi_h}{\partial x}(x(s), y(s))$ and $x'(s) = -\frac{\partial \phi_h}{\partial y}(x(s), y(s))$. So differentiating with the chain rule and making use of the previous expressions yields (dropping the dependence to s to alleviate notations):

$$y''(s) = -\frac{\partial^2 \phi_h}{\partial x^2}\frac{\partial \phi_h}{\partial y} + \frac{\partial^2 \phi_h}{\partial x \partial y}\frac{\partial \phi_h}{\partial x} \tag{18}$$

and:

$$y^{(3)}(s) = -\frac{\partial \phi_h}{\partial x}\left[\frac{\partial^2 \phi_h}{\partial x^2}\frac{\partial^2 \phi_h}{\partial y^2} - \left(\frac{\partial^2 \phi_h}{\partial x \partial y} \right)^2 \right]. \tag{19}$$

We derive similar expressions for the successive derivatives of x, and deduce $|\boldsymbol{f}_\phi|_{g+1,\infty,I} \leq C\|\phi_h\|^{g+1}_{g+1,\infty,S_\delta}$. Hence $|\phi(\boldsymbol{x})| \leq Ch^{g+1}\|\phi\|_{g+1,\infty,S_\delta}\left(1 + \|\phi\|^g_{g+1,\infty,S_\delta}\right)$ so $\epsilon \leq Ch^{g+1}$ which means that the interface is $O(h^{g+1})$ resolved by the subdivision. □

Remark 4.1. However, a locally better resolution of the interface would be appreciable in some situations, for instance cut triangles which are cut close to a node. To remain general, let us consider any $K \in \mathcal{E}_h$. Two of its edges are intersected and the subcell containing their common node is called triangular subcell. This common node is mapped onto the origin of the reference triangle $\hat{K}$ (see Fig. 5). Such a map is moreover chosen such that the first reference coordinate correspond to the largest coordinate $\hat{\lambda}_M$ among the intersection points, while the second reference coordinate is associated with the smallest $\hat{\lambda}_m$.

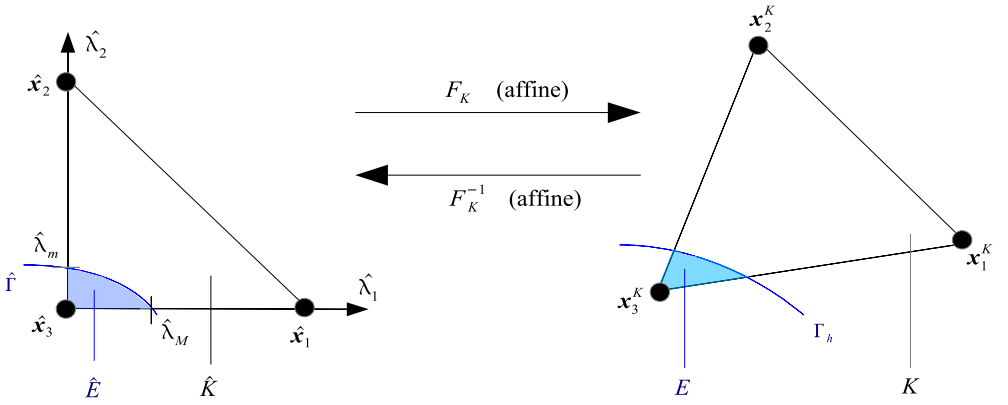

Fig. 5. Intersected triangle.

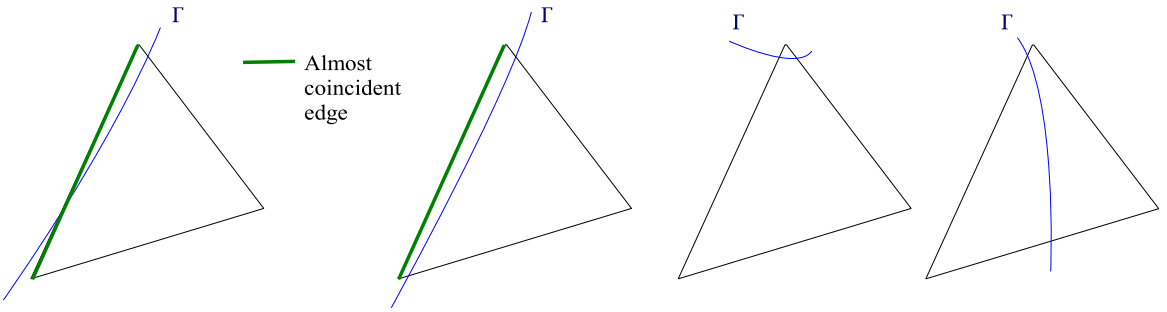

(a) Lengthways intersected triangle whose associated edge is crossed.

(b) Lengthways intersected triangle whose associated edge is not crossed.

(c) Small section but not a lengthways intersected triangle.

(d) Not a lengthways intersected triangle.

Fig. 6. Various configurations of intersected triangles.

The first stage of the approximation may then be consequently improved in $|\phi - I_g\phi|_{0,\infty,\Gamma_h} \leq \hat{\lambda}_M h|\phi - I_g\phi|_{1,\infty,E} \leq C\hat{\lambda}_M h^{g+1}$. The second stage occurs with a triangular subcell E of a characteristic size $\hat{\lambda}_M h$ (see Fig. 5), so in K the interface is locally $O(\hat{\lambda}_M h^{g+1})$-resolved by the subdivision.

With this local property of an improved resolution of the interface, problematic cases are those for which one side has a small area and the interface does not remain in the vicinity of a node, so that no better resolution is available. The characteristic feature of those intersected elements is that the area of the one side is small when compared to the length of the cut interface, hence the terminology developed below:

Definition 4.2. Let $0 < \kappa \ll 1$ be a fixed parameter. A triangle K will be called lengthways intersected if:

$$\exists i \in \{1, 2\}, \quad \frac{\text{meas}(\Omega_i \cap K)}{\text{meas}(\Gamma \cap K)^2} \leq \kappa. \tag{20}$$

For the sake of the demonstration, we use alternative notations from Fig. 5: K is lengthways intersected if:

$$\frac{\min(\hat{\lambda}_m, 1 - \hat{\lambda}_m)}{\hat{\lambda}_M} \leq 2\kappa. \tag{21}$$

To be more practical, for these triangles there is an almost coincident edge with the interface (see Fig. 6(a) and (b)). To be more mathematical, problems will arise from triangulations (family of meshes) for which ratios (20) or (21) are not bounded away from 0 as $h \to 0$. Strictly speaking, we should call lengthways intersected a triangulation, not a triangle.

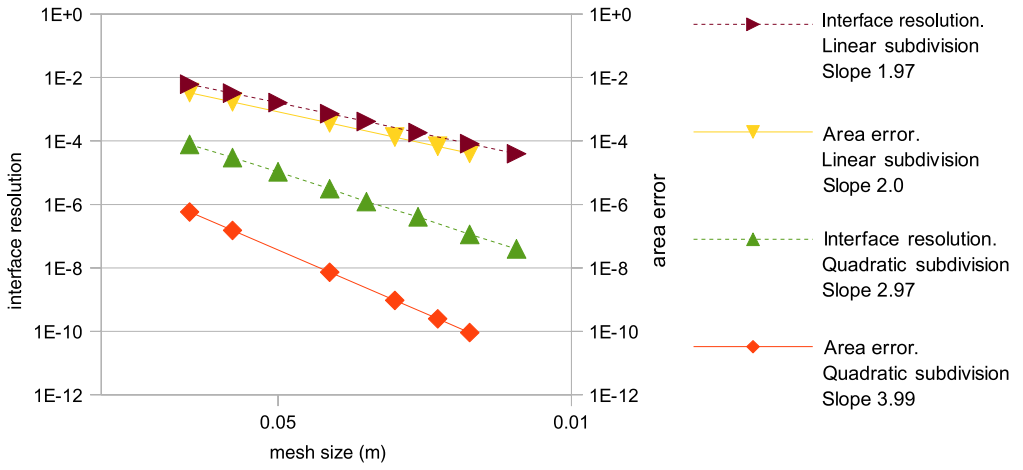

Fig. 7. Typical convergence rates (e.g. for an exponential shape).

4.3. Numerical experiments

The resolution of the interface in the sense of our error measure (Definition 4.1) was computed for various shapes, namely polynomial, exponential, sinusoidal and circular curves. For the sake of comparison with the literature, the classical area error measure is also assessed, which consists of comparing the approximate area on one side of the interface with its analytical value:

$$\text{area error} = \frac{\left|\text{meas}(\Omega_1) - \text{meas}(\Omega_1^h)\right|}{\text{meas}(\Omega_1)}. \tag{22}$$

It is clear from this definition that both error measures should have the same order of convergence, unless a compensation phenomenon occurs on the area error which makes its rate of convergence higher. In accordance with the theory, the observed convergence order for both error measures was always 2 with a linear subdivision. For all shapes but the circle, the interface resolution was observed to converge at order 3 with a quadratic subdivision, as predicted by the theory, while the area error was always 4. The results for the exponential curve are displayed in Fig. 7 as an example. It is still unclear to us what systematic compensation effect is at stake. A super-convergent resolution of the interface was observed for the circle (see Fig. 8), as was already noticed by [15].

5. A priori error estimates depending on geometry description and quadrature

As already pointed out in [6,8], a piecewise linear subdivision yields suboptimal convergence rate with higher-order field interpolation, when the same mesh is used for interpolation and for quadrature. So optimal convergence for curved interfaces relies partly on the representation of the interface geometry, and we shall now quantify this dependence for the strong discontinuity problem presented in Section 2.

5.1. Applying the first Strang lemma

Given that $u \in V$ is discontinuous across Γ and its interpolant $u_h \in V_h$ is discontinuous across Γ_h, $\nabla(u - u_h)$ would not be defined on both of them, thus making difficult the very definition of a H^1-norm. Hence, we chose to define the error as $\|\bar{u} - u_h\|^2_{1,\Omega_1^h \cup \Omega_2^h}$ where $\bar{u}$ is an extension to u to be defined with a discontinuity across Γ_h instead of Γ.

To define such $\bar{u}$, we introduce bounded sets $\bar{\Omega}_i$ which contain all discretizations Ω_i^h from a certain mesh size: $\forall h \leq h_0,\ \bar{\Omega}_i \subset \left(\Omega_i \cup \Omega_i^h\right)$. Let $p \in \{1, 2\}$, we assume that $u \in H^{p+1}(\Omega_1) \times H^{p+1}(\Omega_2)$ and denote u_i its restriction to Ω_i. We may extend u_i to $\bar{u}_i \in H^{p+1}\left(\bar{\Omega}_i\right)$ in a stable way (see Stein [24]). We may then define $\bar{u} \in H^{p+1}(\Omega_1^h) \times H^{p+1}(\Omega_2^h)$ such as $\bar{u}|_{\Omega_i^h} := \bar{u}_i$. The error on the solution is defined as $\|\bar{u} - u_h\|^2_{1,\Omega_1^h \cup \Omega_2^h} = \sum_{i=1,2} \|\bar{u}_i - u_h\|^2_{1,\Omega_i^h}$.

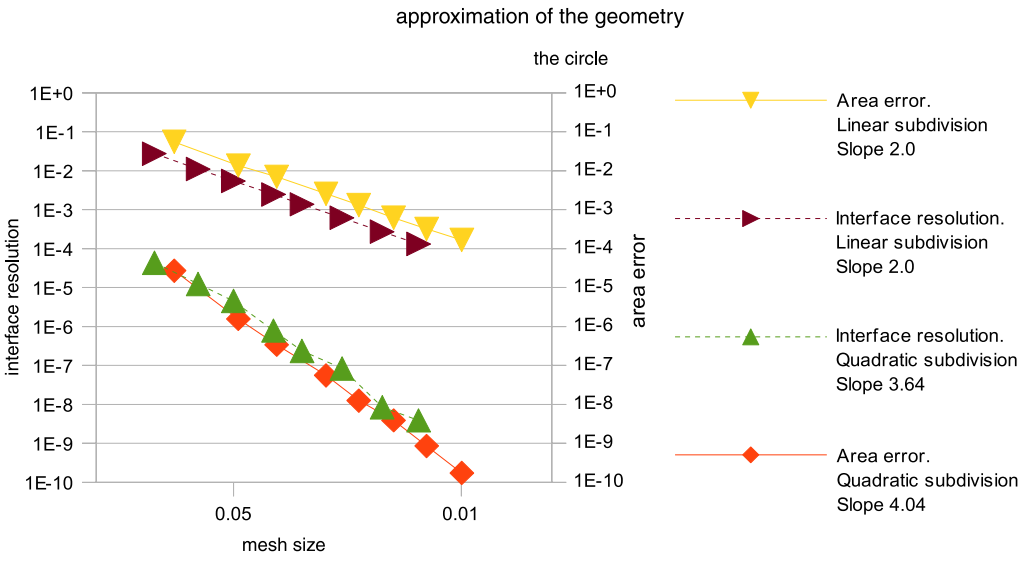

Fig. 8. A superconvergent case: the circle.

Conversely, for a discrete $w_h \in V_h$, we will sometimes be led to use extensions $\bar{w}_h$ being discontinuous across Γ instead of Γ_h. To define them, we note $w_h^i := w_h|_{\Omega_i^h}$. Since it is polynomial on each intersected triangle, we denote $\bar{w}_h^i$ its natural polynomial extension, and build $\bar{w}_h$ by combining the restrictions to Ω_i.

Approximating the operators, the first step is to consider exact integrals but over the approximated domain, which leads to intermediate bilinear and linear forms over $H^1(\Omega_1^h) \times H^1(\Omega_2^h) : \check{a}_h(v, w) := \sum_{i=1,2} \int_{\Omega_i^h} \left(\bar{\boldsymbol{A}}_i \cdot \nabla v\right) \cdot \nabla w dx$ and $\check{l}_h(v) := \sum_{i=1,2} \int_{\Omega_i^h} \bar{f}_i v dx$, where for $i \in \{1, 2\}$, $\bar{\boldsymbol{A}}_i$ and $\bar{f}_i$ are the stable extensions to $\boldsymbol{A}_i$ and f_i related to the Sobolev spaces they respectively belong to.

The second step is the quadrature. On a cut element K, the quadrature scheme is defined over each subcell E. The reference triangle $\hat{K}$ is endowed with an integration scheme whose weights are $\left(\hat{w}_l\right)_{l=1..L}$ and integration points are located at $(\hat{\boldsymbol{b}}_l)_{l=1..L}$. Denoting DF_E the Jacobian matrix of F_E and $J_E := \det(DF_E)$, this yields an integration scheme on each subcell with weights $w_{l,E} = \hat{w}_l J_E(\hat{\boldsymbol{b}}_l)$ and integration points locations $\boldsymbol{b}_{l,E} = F_E(\hat{\boldsymbol{b}}_l)$. Let V_h be the interpolation space (13), the discrete linear and bilinear forms are defined by $\forall (u_h, v_h) \in V_h$:

$$a_h(u_h, v_h) := \sum_{i=1}^{2} \sum_{E \in \Omega_i^h} \sum_{l=1}^{L} w_{l,E} \left(\left[\bar{\boldsymbol{A}}_i \cdot \nabla u_h\right] \cdot \nabla v_h\right) \left(\boldsymbol{b}_{l,E}\right) \tag{23}$$

$$l_h(v_h) := \sum_{i=1}^{2} \sum_{E \in \Omega_i^h} \sum_{l=1}^{L} w_{l,E} \left(\bar{f}_i v_h\right) \left(\boldsymbol{b}_{l,E}\right). \tag{24}$$

The discrete problem then amounts to finding $u_h \in V_h$ such that:

$$\forall v_h \in V_h,\ a_h(u_h, v_h) = l_h(v_h). \tag{25}$$

We recall:

Definition 5.1. The bilinear forms a_h are said to be uniformly V_h-elliptic if there exists $c > 0, \forall v_h \in V_h$, $c\|v_h\|^2_{1,\Omega_1^h \cup \Omega_2^h} \leq a_h(v_h, v_h)$.

A general abstract error estimate then reads:

Proposition 5.1 (*Extension to X-FEM of the Theorem* 4.4.1 *in [19]*)**.** *Assume that the discrete bilinear forms a_h are uniformly V_h-elliptic, there exists a constant C independent of h such that:*

$$\begin{aligned}\|\bar{u}-u_h\|_{1,\Omega_1^h\cup\Omega_2^h} \leq C \inf_{v_h\in V_h}\Bigg\{ & \|\bar{u}-v_h\|_{1,\Omega_1^h\cup\Omega_2^h} \quad \text{(a)} \\ & + \sup_{w_h\in V_h}\frac{|\check{a}_h(v_h,w_h)-a_h(v_h,w_h)|}{\|w_h\|_{1,\Omega_1^h\cup\Omega_2^h}}\Bigg\} + C\sup_{w_h\in V_h}\frac{|\check{l}_h(w_h)-l_h(w_h)|}{\|w_h\|_{1,\Omega_1^h\cup\Omega_2^h}} \quad \text{(b)} \\ & + C\sup_{w_h\in V_h}\frac{|\check{a}_h(\bar{u},w_h)-a(u,\bar{w}_h)|}{\|w_h\|_{1,\Omega_1^h\cup\Omega_2^h}} + C\sup_{w_h\in V_h}\frac{|\check{l}_h(w_h)-l(\bar{w}_h)|}{\|w_h\|_{1,\Omega_1^h\cup\Omega_2^h}} \quad \text{(c)}. \end{aligned} \tag{26}$$

Proof. $\forall (v,w)\in H^1(\Omega_1^h\cup\Omega_2^h)$, by Cauchy–Schwarz and concavity of the square root:

$$\begin{aligned}|\check{a}_h(v,w)| &\leq |\bar{\boldsymbol{A}}|_{0,\infty,\Omega_1\cup\Omega_2}\left(\|\nabla v\|_{\Omega_1^h}\|\nabla w\|_{\Omega_1^h}+\|\nabla v\|_{\Omega_2^h}\|\nabla w\|_{\Omega_2^h}\right)\\ &\leq |\boldsymbol{A}|_{0,\infty,\Omega_1\cup\Omega_2}\left(\sum_{i=1,2}\sum_{j=1,2}\|\nabla v\|_{\Omega_i^h}\|\nabla w\|_{\Omega_j^h}\right)\\ &\leq 2|\boldsymbol{A}|_{0,\infty,\Omega_1\cup\Omega_2}\|v\|_{\Omega_1^h\cup\Omega_2^h}\|w\|_{\Omega_1^h\cup\Omega_2^h}.\end{aligned}$$

Then with a proof strictly identical to [19, 4.4.1], we get:

$$\begin{aligned}\|\bar{u}-u_h\|_{1,\Omega_1^h\cup\Omega_2^h} \leq C\inf_{v_h\in V_h}\Bigg\{ & \|\bar{u}-v_h\|_{1,\Omega_1^h\cup\Omega_2^h}+\sup_{w_h\in V_h}\frac{|\check{a}_h(v_h,w_h)-a_h(v_h,w_h)|}{\|w_h\|_{1,\Omega_1^h\cup\Omega_2^h}}\Bigg\}\\ & + C\sup_{w_h\in V_h}\frac{|\check{a}_h(\bar{u},w_h)-l_h(w_h)|}{\|w_h\|_{1,\Omega_1^h\cup\Omega_2^h}}.\end{aligned}$$

We first decompose:

$$\check{a}_h(\bar{u},w_h)=\left[\check{a}_h(\bar{u},w_h)-a(u,\bar{w}_h)\right]+a(u,\bar{w}_h). \tag{27}$$

And since $a(u,\bar{w}_h)=l(\bar{w}_h)$, we deduce from (27) that:

$$\check{a}_h(\bar{u},w_h)-l_h(w_h)=\left[\check{a}_h(\bar{u},w_h)-a(u,\bar{w}_h)\right]+\left[l(\bar{w}_h)-\check{l}_h(w_h)\right]+\left(\check{l}_h-l_h\right)(w_h) \tag{28}$$

which leads to the result. □

Three kinds of errors appear in estimate (26) of Proposition 5.1. The first one (a) is a rather well-documented interpolation error. The second (b) is the consistency error that we have made by using a quadrature scheme to compute the integrals on the approximated geometry. The third (c) is the consistency error that arises by using operators on the approximated geometry rather than the exact one, the integrals being assumed to be computed exactly.

Because we will need to prove uniform ellipticity for a_h before going any further, let us focus on the integration quantities involved in its expression (23). To this purpose, we recall:

Remark 5.1. Estimates $|DF_K|\leq Ch$ and $|J_K|\leq Ch^2$ hold for any parent element. For $m\in\{1,2\}$, $|D^m F_E|_{0,\infty,\hat{K}}\leq Ch^m$ and for $l\in\{0,1,2\}$, $|J_E|_{l,\infty,\hat{K}}\leq Ch^{l+2}$ hold for any subcell (see [19, Theorem 4.3.3] and its proof). However, while the regularity Assumption (H1) of the parent mesh ensures the inverse properties $|DF_K^{-1}|\leq Ch^{-1}$ and $|J_K^{-1}|\leq Ch^{-2}$, the inverse properties $|DF_E^{-1}|_{0,\infty,E}\leq Ch^{-1}$ and $|J_E^{-1}|_{0,\infty,E}\leq Ch^{-2}$ do not hold for all subcells. To have additional properties for some of them, they should be classified after their shape properties.

Definition 5.2. From the more demanding to the more permissive, we will call:

- Regular, a subcell for which Assumption (H1) holds. For those subcells the inverse properties $|DF_E^{-1}|_{0,\infty,E}\leq Ch^{-1}$ and $|J_E^{-1}|_{0,\infty,E}\leq Ch^{-2}$ hold.

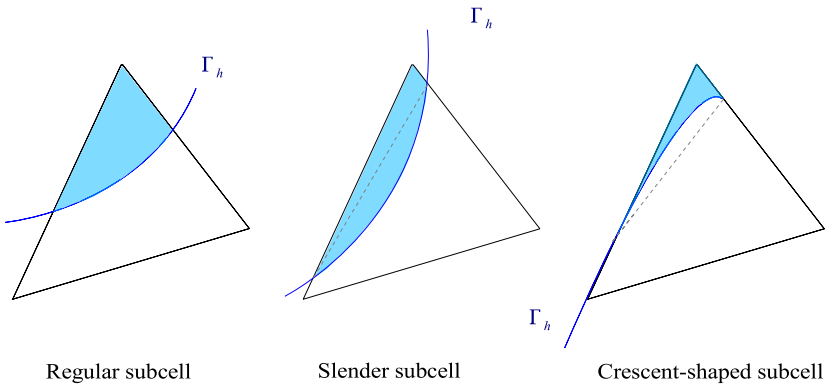

Fig. 9. Regular, slender and crescent-shaped subcells.

- Slender, a non regular subcell E, which, given a constant C independent of h and denoting $J_E^{-1} := \det(DF_E^{-1})$, nevertheless verifies:

$$|J_E^{-1}|_{0,\infty,E}|J_E|_{0,\infty,\hat{K}} \leq C. \tag{29}$$

  Any subcell with no curved edge is either regular or slender.

- Crescent-shaped, a neither regular nor slender subcell.

Again, asymptotically speaking, we should call regular, slender or crescent-shaped families of subcells, but not individuals. Hence, strictly speaking, we call regular a family of subcells of the triangulation for which the ratio in Assumption (H1) remains bounded as $h \to 0$, slender a family for which (29) remains bounded, and crescent-shaped subcells belonging to neither families.

Remark 5.2. In practice, the slenderness property excludes curved subcells which lead to a degenerescence of the angle at the vertex with respect to the similar affine subcell angle (see the third triangle in Fig. 9).

Let us set out the following assumption about quadrature schemes for $k \in \mathbb{N}$:

Assumption (H2, k)**.** The quadrature scheme $(\hat{w}_l, \hat{\boldsymbol{b}}_l)$ is exact for $P_k(\hat{K})$. Further in this paper, we will note (H2, $k = 3$) if the quadrature scheme is exact for $P_3(\hat{K})$ for instance.

We now give a condition under which the approximate bilinear forms are uniformly V_h-elliptic:

Proposition 5.2 (*Extension to X-FEM of [19, Theorem 4.4.2]*)**.** *Let $p = 2$ and $g = 2$. Under Assumptions* (H1)*, (*H2*, $k = 4$) for regular and slender subcells and (*H2*, $k = 6$) for crescent-shaped subcells, the bilinear forms a_h are uniformly V_h-elliptic.*

For $p = 1$ and $g = 1$, uniform ellipticity holds under the Assumptions (H1) and (H2, $k = 0$), and for $p = 2$ and $g = 1$ it holds under Assumptions (H1) and (H2, $k = 2$), the easier proof being left to the reader.

Proof. *Step* 1. Let $K \in \mathcal{E}_h$ and for each side $i \in \{1, 2\}$, let $E \subset \left(K \cap \Omega_i^h\right)$ be a subcell. Let $v_h \in V_h$, and call $p := v_h|_{K\cap\Omega_i^h} \in P_2(K)$. The ellipticity condition on $\boldsymbol{A}$ on the Gauss point number l of E yields:

$$[(\boldsymbol{A} \cdot \nabla p) \cdot \nabla p]\left(\boldsymbol{b}_{l,E}\right) \geq c|\nabla p|^2\left(\boldsymbol{b}_{l,E}\right). \tag{30}$$

The pull-back of p onto the reference parent element will be noted $\hat{p} := p \circ F_K$. Thus, we have for $\boldsymbol{x} \in \left(K \cap \Omega_i^h\right)$, $Dp(\boldsymbol{x}) = D\hat{p}\left(F_K^{-1}(\boldsymbol{x})\right) \cdot DF_K^{-1}$ so since F_K is affine:

$$|Dp(x)|^2 \geq \frac{1}{|DF_K|^2}\left|D\hat{p}\left(F_K^{-1}(x)\right)\right|^2. \tag{31}$$

After (30) and (31), it holds:

$$\sum_{l=1}^{L} w_{l,E}\left[(\boldsymbol{A}\cdot\nabla p)\cdot\nabla p\right]\left(\boldsymbol{b}_{l,E}\right) \geq c\frac{1}{|DF_K|^2}\sum_{l=1}^{L}\left(|D\hat{p}|^2\circ F_K^{-1}\circ F_E(\hat{\boldsymbol{b}}_l)\right)\hat{w}_l J_E(\hat{\boldsymbol{b}}_l). \tag{32}$$

Step 2. *Proof for slender subcells*. We can estimate $J_E(\hat{\boldsymbol{b}}_l) = \frac{1}{J_E^{-1}(\boldsymbol{b}_{l,E})} \geq \left|J_E^{-1}\right|^{-1}_{0,\infty,E}$. Hence:

$$\sum_{l=1}^{L} w_{l,E}\left[(\boldsymbol{A}\cdot\nabla p)\cdot\nabla p\right]\left(\boldsymbol{b}_{l,E}\right) \geq c\frac{\left|J_E^{-1}\right|^{-1}_{0,\infty,E}}{|DF_K|^2}\sum_{l=1}^{L}\left(|D\hat{p}|^2\circ F_K^{-1}\circ F_E(\hat{\boldsymbol{b}}_l)\right)\hat{w}_l. \tag{33}$$

We have $|D\hat{p}|^2\circ F_K^{-1}\circ F_E \in P_4(\hat{K})$ which thanks to (H2, $k=4$) allows the conversion of right-side member into an exact integral that may be estimated in the following way:

$$\begin{aligned}\sum_{l=1}^{L}\hat{w}_l|D\hat{p}|^2\left(F_K^{-1}\circ F_E(\hat{\boldsymbol{b}}_l)\right) &= \int_{\hat{K}}\left(|D\hat{p}|^2\circ F_K^{-1}\circ F_E(\hat{\boldsymbol{x}})\right)d\hat{x}\\ &\geq |J_E|^{-1}_{0,\infty,E}J_K\int_{\hat{E}}|D\hat{p}|^2 d\hat{x}\end{aligned} \tag{34}$$

where we have noted $\hat{E} \coloneqq F_K^{-1}(E) \subset \hat{K}$ (see Fig. 5). Combining (33) and (34), the definition (29) of slender subcells, and the classical estimates $|\hat{p}|^2_{1,\hat{E}} \geq cJ_K^{-1}|DF_K|^2|p|^2_{1,E}$ (see [19, Theorem 4.3.2]), we may conclude:

$$\sum_{l=1}^{L} w_{l,E}\left[(\boldsymbol{A}\cdot\nabla p)\cdot\nabla p\right]\left(\boldsymbol{b}_{l,E}\right) \geq c|p|^2_{1,E}. \tag{35}$$

Step 3. *Proof for crescent-shaped subcells*. Since F_K is affine so is F_K^{-1}, and $F_E \in P_2(\hat{K})$ which implies:

$$J_E\left(|D\hat{p}|^2\circ F_K^{-1}\circ F_E\right) \in P_6(\hat{K}). \tag{36}$$

Thanks to (36) and (H2, $k=6$), the right-side member of (32) may be converted into an exact integral, which after a change of integration domain gives:

$$\sum_{l=1}^{L} w_{l,E}\left[(\boldsymbol{A}\cdot\nabla p)\cdot\nabla p\right]\left(\boldsymbol{b}_{l,E}\right) \geq c\frac{1}{|DF_K|^2}J_K|\hat{p}|^2_{1,\hat{E}}. \tag{37}$$

By the same classical estimates $|\hat{p}|^2_{1,\hat{E}} \geq cJ_K^{-1}|DF_K|^2|p|^2_{1,E}$, we may conclude:

$$\sum_{l=1}^{L} w_{l,E}\left[(\boldsymbol{A}\cdot\nabla p)\cdot\nabla p\right]\left(\boldsymbol{b}_{l,E}\right) \geq c|p|^2_{1,E}. \tag{38}$$

Step 4. Summing up (35) over E yields:

$$\exists c>0,\ \forall v_h\in V_h,\quad a_h(v_h,v_h) \geq c|v_h|^2_{1,\Omega_1^h\cup\Omega_2^h}. \tag{39}$$

We may now prove the same property with the norm instead of the semi-norm following the proof of [19, Theorem 4.4.2]. Applying the Poincaré inequality over $\bar{\Omega}_i$ to Stein extensions of v_h, we may find a constant independent of h such as $\forall v \in V_h, \|v\|_{1,\Omega_1^h\cup\Omega_2^h} \leq C|v|_{1,\Omega_1^h\cup\Omega_2^h}$ which yields the final result $\exists c>0, \forall v_h\in V_h, a_h(v_h,v_h) \geq c\|v_h\|^2_{1,\Omega_1^h\cup\Omega_2^h}$. □

Having established a condition which ensures that the assumption of the abstract error estimate (26) holds, we take to estimating its different terms. Let us start with the interpolation error (a) in (26). As it is well-documented in the literature, we stick to the essential.

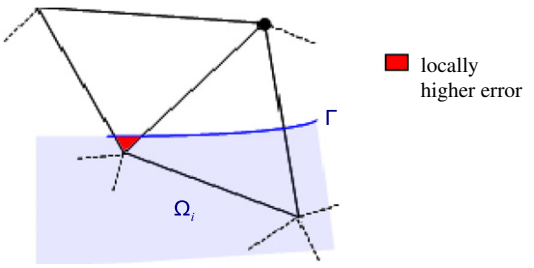

Fig. 10. Situation responsible for local high errors.

Definition 5.3 (*[10,12,25]*)**.** Let $p \in \{1,2\}$ be the interpolation order, let $u \in H^{p+1}(\Omega_1 \cup \Omega_2)$, we introduce an interpolation operator Π_h onto V_h by $\Pi_h u := \sum_{l\in\mathcal{N}_h} a_l N_l + \sum_{l\in\mathcal{K}_h} b_l N_l H$, where a_i, b_i are given by ($\boldsymbol{x}_i$ being the position of the node associated with N_i):

- if $l \in \mathcal{N}_h \setminus \mathcal{K}_h$ then $a_l := u(\boldsymbol{x}_l)$,
- if $l \in \mathcal{K}_h$ then: $\begin{cases} a_l := \frac{1}{2}\left(u_i(\boldsymbol{x}_l) + \bar{u}_j(\boldsymbol{x}_l)\right) \\ b_l := \frac{1}{2}(-1)^i\left(u_i(\boldsymbol{x}_l) - \bar{u}_j(\boldsymbol{x}_l)\right) \end{cases}$ where $\boldsymbol{x}_l \in \Omega_i^h$ and $j := 3 - i$.

Note that Definition 5.3 implies that if I_p is the nodal interpolation operator, then $\Pi_h u|_{\Omega_i^h} = I_p \bar{u}_i$. The definition is consistent since $H^2(\Omega_1 \cup \Omega_2) \subset C^0(\Omega_1 \cup \Omega_2)$.

Proposition 5.3. *Let $p \in \{1,2\}$, let $u \in H^{p+1}(\Omega_1 \cup \Omega_2)$, the following interpolation estimate holds:*

$$\|\bar{u} - \Pi_h u\|_{1,\Omega_1^h \cup \Omega_2^h} \leq Ch^p \|u\|_{p+1,\Omega_1\cup\Omega_2}. \tag{40}$$

Proof. The reader is referred to [10,12] for the case where $p = 1$. For $p = 2$, the regularity of the parent elements and the stability of the extension give:

$$\|\bar{u}_i - I_2\bar{u}_i\|_{1,\Omega_i^h} \leq Ch^p \|\bar{u}_i\|_{p+1,\bar{\Omega}_i} \leq Ch^p \|u_i\|_{p+1,\Omega_i}. \tag{41}$$

Summing up the results yields the desired property by definition of Π_h. □

Note that the properties above say nothing about punctual values of the gradient (that in so say in the sense of the norm of $W^{1,\infty}(\Omega_i)$): let us first illustrate how a classical (naive) estimate for this norm indeed fails to prove local convergence for small sections. Take as the exact solution a polynomial, but with an order $q > p$ too high to be spanned by the basis. Let $K \in \mathcal{E}_h$ be a triangle cut on a small section, so that $\frac{\text{meas}(K\cap\Omega_i)}{\text{meas}(K)} = \kappa \ll 1$. The equivalence of all norms on $P_q(K \cap \Omega_i)$ yields $\|u - \Pi_h u\|_{1,\infty,\Omega_i\cap K} \leq C\kappa^{-1/2}h^{-1}\|u - \Pi_h u\|_{1,\Omega_i\cap K}$. We may then use the classical estimate from [10,12,26] $\|u - \Pi_h u\|_{1,\ K\cap\Omega_i} \leq Ch^p\|\bar{u}_i\|_{p+1,K}$. The equivalence of norms over $P_q(K)$ finally yields:

$$\|u - \Pi_h u\|_{1,\infty,\Omega_i\cap K} \leq C\kappa^{-1/2}h^{p+1}\|\bar{u}_i\|_{p+1,K}. \tag{42}$$

Using quasi-interpolation operators improves the classical estimates of [12] into $\|u - \Pi_h u\|_{1,K\cap\Omega_i} \leq Ch^p \|u_i\|_{p+1,K\cap\Omega_i}$ *except for an alternation of small and large sections*, such as that represented in Fig. 10. The analysis has not been reported here since quasi-interpolation operators are beyond the scope of this paper.

In practice, the phenomenon is familiar to X-FEM users, where incorrect values are often noticed at small sections. However, the very fact that they occur only on small areas ensures that the (theoretically proven) H^1-convergence is not affected. So the wise user will either have engineering quantities of interest defined by integrals, or drop those small sections when looking for maximal stress or strains.

5.2. About the quadrature rules in the subcells

We shall handle consistency errors (b) in (26), arising from using a quadrature to evaluate the integrals. The point of this section is to prove that they do not yield suboptimal rates of convergence. In a nutshell, the paradigm of the next two propositions is to rely on the fact that interpolation occurs on affine parent elements whose mapping, Jacobian

and their inverse are well-known, and the fact that the subcells have polynomial geometrical quantities (mappings and Jacobian). The idea is then to increase the quadrature order to include the description of those geometrical quantities as the shape of the subcells gets *worse*.

To explain it the other way round, for a uniform material and the case $p = 2$, a scheme correctly integrating P_6 would be exact as it corresponds to the maximal order obtained taking into account geometrical and interpolation effects. As the shape of the subcells gets more *regular*, some contributions due to geometrical effects become very small, and may be neglected while keeping the integration error reasonably low.

Let $\hat{\varphi}$ be a continuous function over $\hat{K}$, we define a quadrature error by $\hat{\Delta}(\hat{\varphi}) := \int_{\hat{K}} \hat{\varphi}\, d\hat{x} - \sum_{l=1}^{L} \hat{w}_l \hat{\varphi}(\hat{\boldsymbol{b}}_l)$. In the same way, the quadrature error on a subcell $E \in \mathcal{S}_h$ of a continuous function over $\hat{E}$ is $\Delta_E(\varphi) := \int_E \varphi\, dx - \sum_{l=1}^{L} w_{l,E} \varphi(\boldsymbol{b}_{l,E})$. It is estimated by:

Proposition 5.4 (*Extension to X-FEM of [19, Theorem 4.4.4]*)**.** *Let $p = 2$ and $g = 2, E \in \mathcal{S}_h, K \in \mathcal{E}_h$ such that $E \subset K$. Under Assumptions* (H1)*, (*H2*, k = 7) and $A \in W^{2,\infty}(E)$ for crescent-shaped subcells, (*H2*, k = 5) and $A \in W^{4,\infty}(E)$ for slender subcells, (*H2*, k = 3) and $A \in W^{2,\infty}(E)$ for regular subcells; we have* $\forall (p, p') \in (P_2(E))^2 \left|\Delta_E\left(\left(\boldsymbol{A}\cdot\nabla p'\right)\cdot\nabla p\right)\right| \leq Ch^2 \|A\|_{2,\infty,E} \|p'\|_{2,E} |p|_{1,E}$.

In case $p = 1$ and $g = 1$, Assumptions (H1), (H2, $k = 0$) and $A \in W^{1,\infty}(E)$ ensure a quadrature consistency error (whose easier demonstration is left to the reader): $\forall (p, p') \in (P_1(E))^2, \left|\Delta_E\left(\left(\boldsymbol{A}\cdot\nabla p'\right)\cdot\nabla p\right)\right| \leq Ch\|A\|_{1,\infty,E}\|p'\|_{1,E}|p|_{1,E}$.

Proof. *Step* 1. Let $(\boldsymbol{e}_1, \boldsymbol{e}_2)$ be an orthonormal basis of the plane, let $\partial_i v := Dv \cdot \boldsymbol{e}_i$, for $(i, j) \in \{1, 2\}^2$, we have:

$$\Delta_E\left(A_{ij}\partial_i p' \partial_j p\right) = \hat{\Delta}\left[\left(A_{ij}\circ F_E\right)\left(\partial_i p' \circ F_E\right)\left(\partial_j p \circ F_E\right) J_E\right].$$

Introducing the pullback with respect to the parent element $\hat{p} := p \circ F_K$ yields $\partial_j p\,(x) = D\hat{p}\left(F_K^{-1}(x)\right)\cdot DF_K^{-1}\cdot e_j$. Let us call $\boldsymbol{e}_{j'} := \frac{DF_K^{-1}\cdot\boldsymbol{e}_j}{|DF_K^{-1}\cdot\boldsymbol{e}_j|}$, then this may be reformulated into $\partial_j p\,(x) = \left|DF_K^{-1}\cdot\boldsymbol{e}_j\right|\ \partial_{j'}\hat{p}\left(F_K^{-1}(x)\right)$. Since $\left|DF_K^{-1}\cdot\boldsymbol{e}_j\right| \leq |DF_K^{-1}|$, we have:

$$\Delta_E\left(A_{ij}\partial_i p'\partial_j p\right) \leq |DF_K^{-1}|^2 \hat{\Delta}\left[\left(A_{ij}\circ F_E\right)\left(\partial_{i'}\hat{p}'\circ F_K^{-1}\circ F_E\right)\left(\partial_{j'}\hat{p}\circ F_K^{-1}\circ F_E\right) J_E\right]. \tag{43}$$

Step 2: *Proof for crescent-shaped subcells*. To alleviate notations, we denote $\hat{w} := \left(\partial_{i'}\hat{p}'\right)\circ F_K^{-1}\circ F_E\left(\partial_{j'}\hat{p}\right)\circ F_K^{-1}\circ F_E J_E$, $\hat{a} := a\circ F_E := A_{ij}\circ F_E$ and notice that $\hat{w} \in P_6(\hat{K})$. Hence with (H2, $k = 7$) the continuous linear form $\hat{\varphi} \to \hat{\Delta}\left(\hat{\varphi}\hat{w}\right)$ assessing the quadrature error vanishes over the space $P_1(\hat{K})$, so the Bramble–Hilbert lemma [19, Theorem 4.1.3] asserts that:

$$\exists C, \quad \hat{\Delta}\left(\hat{a}\hat{w}\right) \leq C|\hat{a}|_{2,\infty,\hat{K}}|\hat{w}|_{0,\hat{K}}. \tag{44}$$

The second term is evaluated by $|\hat{w}|^2_{0,\hat{K}} \leq |J_E|_{0,\infty,\hat{K}} J_K |\partial_{i'}\hat{p}'\partial_{j'}\hat{p}|^2_{0,\hat{E}}$. By virtue of the Cauchy–Schwarz inequality and $|\hat{p}|_{1,\hat{E}} \leq J_K^{-1/2}|DF_K|\,|p|_{1,E}$, we assess:

$$|\hat{w}|_{0,\hat{K}} \leq |J_E|^{1/2}_{0,\infty,\hat{K}} J_K^{-1/2}|DF_K|^2|p|_{1,E}|p'|_{1,E}. \tag{45}$$

Moreover $D^2\hat{a} = D^2\left(a\circ F_E\right) = DF_E^T\cdot D^2 a\cdot DF_E + Da\cdot D^2F_E$, which given that $|DF_E| \leq Ch$ and $|D^2F_E| \leq Ch^2$ yields:

$$|\hat{a}|_{2,\infty,\hat{K}} \leq Ch^2\|a\|_{2,\infty,E}. \tag{46}$$

Assumption (H1) implies that $|DF_K|^2 J_K^{-1/2}|DF_K^{-1}|^2 \leq Ch^{-1}$, which combined with $|J_E|^{1/2}_{0,\infty,\hat{K}} \leq Ch$ and Eqs. (44)–(46) yields:

$$\left|\Delta_E\left(a\partial_i p'\partial_j p\right)\right| \leq Ch^2\|a\|_{2,\infty,E}|p|_{1,E}|p'|_{1,E}. \tag{47}$$

Step 3: *Proof for slender subcells*. Starting from Eq. (43) we set $\hat{v} := \left(\partial_{i'}\hat{p}'\right) \circ F_K^{-1} \circ F_E \in P_2(\hat{K})$, $\hat{u} := \left(\partial_{j'}\hat{p}\right) \circ F_K^{-1} \circ F_E \in P_2(\hat{K})$ and $\hat{b} := (a \circ F_E)\, J_E$. Given (H2, $k = 5$), the continuous linear form $\hat{\varphi} \to \hat{\Delta}\left(\hat{\varphi}\hat{u}\right)$ vanishes over $P_3(\hat{K})$. Using the Bramble–Hilbert lemma and the Leibniz rule for derivating a product yields:

$$\left|\hat{\Delta}\left(\hat{b}\hat{v}\hat{u}\right)\right| \leq C\left(\sum_{j=0}^{2} |\hat{b}|_{4-j,\infty,\hat{K}} |\hat{v}|_{j,\hat{K}}\right) |\hat{u}|_{0,\hat{K}}. \tag{48}$$

For $j \in \{0, 1\}$, we have:

$$\begin{aligned} |\hat{v}|_{j,\hat{K}} &\leq J_K^{1/2} |DF_E|^j_{0,\infty,\hat{K}} |J_E^{-1}|^{1/2}_{0,\infty,\hat{K}} |DF_K^{-1}|^j |\hat{p}'|_{1+j,\hat{E}} \\ &\leq |DF_E|^j_{0,\infty,\hat{K}} |J_E^{-1}|^{1/2}_{0,\infty,\hat{K}} |DF_K^{-1}|^j |DF_K|^{1+j} \|p'\|_{1+j,E}. \end{aligned} \tag{49}$$

Since F_K is affine and $\hat{p}' \in P_2(\hat{E})$:

$$|\hat{v}|_{2,\hat{K}} \leq |J_E^{-1}|^{1/2}_{0,\infty,\hat{K}} |D^2 F_E|_{0,\infty,\hat{K}} |DF_K|^2 \, |DF_K^{-1}| \, \|p'\|_{2,E}. \tag{50}$$

Moreover: $|\hat{b}|_{4-j,\infty,\hat{K}} \leq 6 \sum_{l=0}^{\min\{4-j,2\}} |\hat{a}|_{4-j-l,\infty,\hat{K}} |J_E|_{l,\infty,\hat{K}}$. Given that $F_E \in P_2(\hat{K})$ and $|D^l F_E| \leq Ch^l$ for $l \in \{0, 1, 2\}$, one could easily prove $|\hat{a}|_{4-j-l,\infty,\hat{K}} \leq Ch^{4-j-l}\|a\|_{4,\infty,E}$. Since $J_E \in P_2(\hat{K})$, we get $|J_E|_{l,\infty,\hat{K}} \leq C|J_E|_{0,\infty,\hat{K}}$ by virtue of the equivalence of all norms over $P_2(\hat{K})$, which leads to:

$$|\hat{b}|_{4-j,\infty,\hat{K}} \leq C|J_E|_{0,\infty,\hat{K}} h^{2-j} \|a\|_{4,\infty,E}. \tag{51}$$

Combining (48)–(51), using the estimates of Remark 5.1 and the definition (29) of a slender subcell, it follows that:

$$\left|\hat{\Delta}\left(\hat{b}\hat{v}\hat{u}\right)\right| \leq Ch^4 \|p'\|_{2,E} |p|_{1,E} \|a\|_{4,\infty,E}. \tag{52}$$

Given (43) and (52), we may conclude:

$$\Delta_E\left(a\partial_i p' \partial_j p\right) \leq Ch^2 \|p'\|_{2,E} |p|_{1,E} \|a\|_{4,\infty,E}. \tag{53}$$

Step 4: *Proof for regular subcells*. The proof follows the same line than in Step 3 but for linear forms vanishing over $P_1(\hat{K})$ instead of $P_3(\hat{K})$. Eq. (48) becomes:

$$\left|\hat{\Delta}\left(\hat{b}\hat{v}\hat{u}\right)\right| \leq C\left(\sum_{j=0}^{2} |\hat{b}|_{2-j,\infty,\hat{K}} |\hat{v}|_{j,\hat{K}}\right) |\hat{u}|_{0,\hat{K}}. \tag{54}$$

Again, the derivatives of $\hat{b}$ may be estimated by a Leibniz formula, but this time a classical estimate $|J_E|_{l,\infty,\hat{K}} \leq Ch^{l+2}$ is used to estimate the derivative of the Jacobian. Along with Remark 5.1, it holds:

$$|\hat{b}|_{2-j,\infty,\hat{K}} \leq Ch^{4-j} \|a\|_{2,\infty,E}. \tag{55}$$

This time the inverse properties of Definition 5.2 may be used to evaluate (49) and (50) in $|\hat{v}|_{j,\infty,\hat{K}} \leq Ch^j \|p'\|_{2,E}$, which leads to (52) and (53). □

Remark 5.3. Note that the property $|J_E|_{l,\infty,\hat{K}} \leq Ch^l |J_E|_{0,\infty,\hat{K}}$ would have improved estimate (51) by two orders and decreased by as much the required quadrature scheme, but we failed to prove it for all slender subcells.

Having evaluated the quadrature error in the integral defining the stiffness matrix, we shall now estimate the one defining the volume forces:

Proposition 5.5 (*Generalization to X-FEM of [19, Theorem 4.4.5]*)**.** *Let $p = 2$ and $g = 2$, $E \in \mathcal{S}_h$, $K \in \mathcal{T}_h$ such that $E \subset K$ and assume that $f \in W^{1,\infty}(E)$. Under Assumptions* (H1)*,* (H2*, $k = 6$*) for crescent-shaped or slender subcells and (*H2*, $k = 4$*) for regular subcells; we have $\forall p \in P_2(E) : |\Delta_E(fp)| \leq Ch^2 \|p\|_{0,E} \|f\|_{1,\infty,E}$.*

In case $p = 1$ and $g = 1$, under the Assumptions (H1), (H2, $k = 0$) and $f \in L^\infty(E)$, we have $\forall p \in P_1(E)\, |\Delta_E(fp)| \leq Ch\|p\|_{0,E}\|f\|_{0,\infty,E}$. The proof is left to the reader.

Proof. *Step* 1: *proof for crescent-shaped or slender subcells.*

The proof is analogous to that of Proposition 5.4, Step 2. We have $\Delta_E(fp) = \hat{\Delta}\left(\hat{f}\hat{v}\right)$ with $\hat{f} \coloneqq f \circ F_E$ and $\hat{v} \coloneqq (p \circ F_E)\, J_E$. Since $\hat{v} \in P_6(\hat{K})$, by (H2, $k = 6$) the continuous linear form $\hat{\varphi} \to \hat{\Delta}\left(\hat{\varphi}\hat{v}\right)$ vanishes over $P_0(\hat{K})$, so after the Bramble–Hilbert lemma:

$$\begin{aligned}\left|\hat{\Delta}\left(\hat{f}\hat{v}\right)\right| &\leq C|\hat{f}|_{1,\infty,\hat{K}}|\hat{v}|_{0,\hat{K}}\\ &\leq C|DF_E|_{0,\infty,\hat{K}}|J_E|^{1/2}_{0,\infty,\hat{K}}|p|_{0,E}\|f\|_{1,\infty,E}\\ &\leq Ch^2|p|_{0,E}\|f\|_{1,\infty,E}. \end{aligned} \tag{56}$$

Step 2: *proof for regular subcells*. We have $\Delta_E(fp) = \hat{\Delta}(\hat{f}\hat{v})$ but with $\hat{f} \coloneqq (f \circ F_E)\, J_E$ and $\hat{v} \coloneqq p \circ F_E$. Since $\hat{v} \in P_4(\hat{K})$ and (H2, $k = 4$), the continuous linear form $\hat{\varphi} \to \hat{\Delta}\left(\hat{\varphi}\hat{v}\right)$ vanishes over $P_0(\hat{K})$. The Bramble–Hilbert lemma gives $\left|\hat{\Delta}(\hat{f}\hat{v})\right| \leq \hat{C}|\hat{f}|_{1,\infty,\hat{K}}|\hat{v}|_{0,\hat{K}}$.

Then $|\hat{f}|_{1,\infty,\hat{K}} \leq |DF_E|\,|f|_{1,\infty,E}|J_E|_{0,\infty,\hat{K}} + |f|_{0,\infty,E}|J_E|_{1,\infty,\hat{K}}$ and $|\hat{v}|_{0,\hat{K}} \leq |J_E^{-1}|^{1/2}_{0,\infty,\hat{K}}|p|_{0,E}$, and we get the result after the properties of Definition 5.2. □

5.3. Geometry influence on the error

We now focus on consistency error (c) in (26), which is the most interesting, and arises by approximating the geometry. Excluding lengthways intersected elements from the proof, we show that (c) is expressed as $\epsilon h^{-1/2}$, ϵ being the geometrical error measure of Section 4. However, the numerical experiments in Section 6 and the extended proof in the Appendix C suggest that the estimates holds even for those elements in practice. A recap of all results then yields the final estimates:

Theorem 5.1 (*Inspired from [20, Section 4.4]*)**.** *Assume* (H1) *and a quadrature scheme adapted to the regularity properties of the subcells (see Propositions* 5.2, 5.4 *and* 5.5 *for full details). The interface is supposed to be ϵ-resolved by the subdivision, with no lengthways intersected triangles. Suppose $A \in W^{2,\infty}(\Omega_1 \cup \Omega_2)$, $f \in W^{1,\infty}(\Omega_1 \cup \Omega_2)$ and $u \in H^{p+1}(\Omega_1 \cup \Omega_2)$, then the following error estimate holds:*

$$\begin{aligned}\|\bar{u} - u_h\|_{1,\Omega_1^h \cup \Omega_2^h} \leq\ & Ch^p\left[\|u\|_{p+1,\Omega}\left(1 + \|A\|_{p,\infty,\Omega}\right) + \|f\|_{p-1,\infty,\Omega}\right]\\ &+ C\frac{\epsilon}{h^{1/2}}\left(\|f\|_{0,\infty,\Omega} + \|u\|_{1,\infty,\Omega}\|A\|_{0,\infty,\Omega}\right). \end{aligned} \tag{57}$$

Proof. *Step* 1: *Recap the results*. Due to Proposition 5.2, the approximate bilinear forms a_h are uniformly V_h-elliptic, so the abstract error estimate (26) of Proposition 5.1 may be used. By letting $v_h = \Pi_h u$ in this estimate, we may estimate the interpolation error ((26)(a)) by Proposition 5.3. Besides, all requirements are met to use the consistency estimate of Proposition 5.4, which summing up the results over all subcells and using the stability properties of Π_h gives (in case $p = 2$):

$$\frac{\left|a_h(\Pi_h u, w_h) - \breve{a}_h(\Pi_h u, w_h)\right|}{\|w_h\|_{1,\Omega_1^h \cup \Omega_2^h}} \leq Ch^2\|u\|_{2,\Omega_1\cup\Omega_2}\|A\|_{2,\infty,\Omega_1\cup\Omega_2}. \tag{58}$$

By the same token, the second term in ((26)(b)) is estimated by Proposition 5.5.

Step 2: The error due to the change of domain. Let us estimate terms ((26)(c)), which are due to the use of a non-conforming finite element method because of the change in domain. Appealing to the Section 4.4 of [20], the last two terms may be written as integrals over the skin (the part of Ω_i which does not belong to Ω_i^h and conversely):

$$\breve{a}_h(\bar{u}, w_h) - a(u, \bar{w}_h) = \sum_{i=1}^{2}\left(\int_{\Omega_i^h \setminus \Omega_i} A\nabla\bar{u}_i\nabla w_h dx - \int_{\Omega_i \setminus \Omega_i^h} A\nabla u_i\nabla\bar{w}_h dx\right). \tag{59}$$

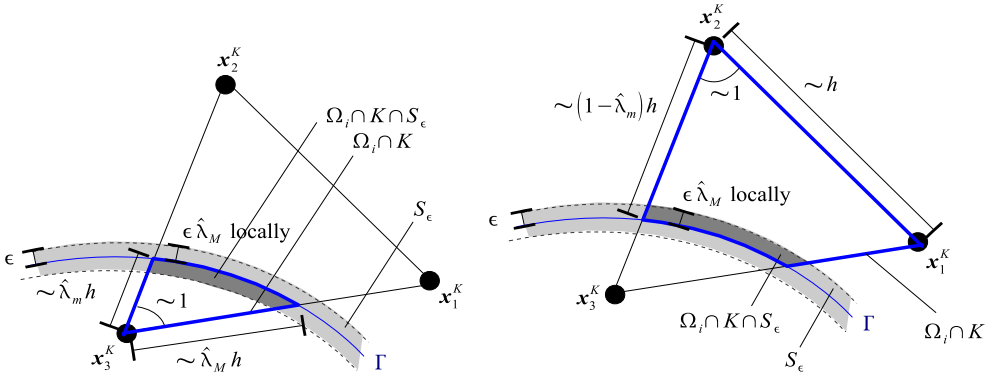

(a) Side of the triangular subcell. (b) Other side.

Fig. 11. Intersected triangle and measures of interest.

The Cauchy–Schwarz inequality on the above equation yields (as a reminder, S_ϵ is the 2ϵ-wide strip centered on Γ, see Fig. 11):

$$\left|\check{a}_h(\bar{u}, w_h) - a(u, \bar{w}_h)\right| \leq \mathrm{meas}(S_\epsilon)^{1/2} \|A\|_{0,\infty,\Omega} \Big(\|u\|_{1,\infty,\Omega_1\cup\Omega_2} |\bar{w}_h|_{1,S_\epsilon\cap(\Omega_1\cup\Omega_2)} + \|\bar{u}\|_{1,\infty,\Omega_1^h\cup\Omega_2^h} |w_h|_{1,S_\epsilon\cap(\Omega_1^h\cup\Omega_2^h)} \Big). \tag{60}$$

It is obvious that $\mathrm{meas}(S_\epsilon) = O(\epsilon)$, and we may use Berger's lemma (see [20, Lemma 2.2]), which states that the integral of a polynomial function over a subdomain of its original definition domain is controlled by the ratio of the areas multiplied by the integral over the whole domain:

$$\|\bar{w}_h\|^2_{1,S_\epsilon\cap\Omega_i\cap K} \leq C \frac{\mathrm{meas}(S_\epsilon \cap \Omega_i \cap K)}{\mathrm{meas}(\Omega_i \cap K)} \|\bar{w}_h\|^2_{1,\Omega_i\cap K}. \tag{61}$$

In order to estimate the ratio, equivalent measures to the quantities of interest are represented in Fig. 11:

- with Assumption (H1) that the mesh is regular, the angles of the parent triangle K are bounded away from zero,
- the interface Γ is globally ϵ-resolved by the subdivision, but as we have seen in Remark 4.1, we have a better precision when considering the intersection with K only: it is locally $\epsilon\hat{\lambda}_M$-resolved by the subdivision,
- the length of this intersection $\Gamma \cap K$ is equivalent to $\hat{\lambda}_M h$.

We may now evaluate the area of the dark gray strip in Fig. 11, as we have estimated its width and length respectively from the last two points. It reads $\mathrm{meas}(S_\epsilon \cap \Omega_i \cap K) \leq C(\epsilon\hat{\lambda}_M)\hat{\lambda}_M h$. If i is the side of the triangular subcell (see Fig. 11(a)), then it comes $\mathrm{meas}(\Omega_i \cap K) \geq c(\hat{\lambda}_M h)\hat{\lambda}_m h$. Otherwise (see Fig. 11(b)), we may assert $\mathrm{meas}(\Omega_i \cap K) \geq c(1-\hat{\lambda}_m)h^2 \geq c(1-\hat{\lambda}_m)\hat{\lambda}_M h^2$. Hence, it comes:

$$\frac{\mathrm{meas}(S_\epsilon \cap \Omega^i \cap K)}{\mathrm{meas}(\Omega^i \cap K)} \leq C \frac{\epsilon}{h} \frac{\hat{\lambda}_M}{\min\{\hat{\lambda}_m, 1-\hat{\lambda}_m\}}. \tag{62}$$

At this stage, we come across Definition 4.2 of lengthways intersected triangles. Indeed, for triangles which are not lengthways intersected, Definition 4.2 states that $\frac{\hat{\lambda}_M}{\min\{\hat{\lambda}_m, 1-\hat{\lambda}_m\}}$ is bounded, so that by combining (61) with (62):

$$\|\bar{w}_h\|^2_{1,S_\epsilon\cap\Omega_i\cap K} \leq C \frac{\epsilon}{h} \|\bar{w}_h\|^2_{1,\Omega_i\cap K}. \tag{63}$$

As a remark, we may still derive this property on the side of the intersection with the larger area (Fig. 11(b)) for lengthways intersected triangles. On the contrary, on the smaller side (Fig. 11(a)), no such property can be established. Then, decomposing $\|\bar{w}_h\|^2_{1,\Omega_i\cap K} \leq \|\bar{w}_h\|^2_{1,(\Omega_i\setminus S_\epsilon)\cap K} + \|\bar{w}_h\|^2_{1,\Omega_i\cap S_\epsilon\cap K}$, and making use of (63), we have $\|\bar{w}_h\|^2_{1,\Omega_i\cap K} \leq \|w_h\|^2_{1,\Omega_i^h\cap K} + C\frac{\epsilon}{h}\|\bar{w}_h\|^2_{1,\Omega_i\cap K}$. Given Theorem 4.1, ϵ is at least a $O(h^2)$, so for h small enough, it comes:

$$\|\bar{w}_h\|_{1,\Omega_i\cap K} \leq C \|w_h\|_{1,\Omega_i^h\cap K}. \tag{64}$$

Table 1
Expected rates of convergence as a function of the displacement, geometry and quadrature according to (58).

Displacement	Representation order g of the geometry	Assumed accuracy of the quadrature scheme	Convergence order of the interface resolution ϵ	Consistency geometry: order of $\epsilon h^{-1/2}$	Displacement interpolation error rate p	Energy error rate
P1	1	1	2	1.5	1	1
P2	1	2	2	1.5	2	1.5
P2	2	2	3	2.5	2	2

Combining (64) and (63), summing up over all intersected elements, and replacing the result in (60), we obtain:

$$\frac{\left|\check{a}_h\left(\bar{u}, w_h\right) - a\left(u, \bar{w}_h\right)\right|}{\|w_h\|_{1,\Omega_1^h \cup \Omega_2^h}} \leq C \frac{\epsilon}{h^{1/2}} \|A\|_{0,\infty,\Omega} \|u\|_{1,\infty,\Omega_1 \cup \Omega_2}. \tag{65}$$

Following the very same procedure, one shows that:

$$\frac{\left|l(\bar{w}_h) - \check{l}_h(w_h)\right|}{\|w_h\|_{1,\Omega_1^h \cup \Omega_2^h}} \leq C \frac{\epsilon}{h^{1/2}} \|f\|_{0,\infty,\Omega} \tag{66}$$

which ends the proof. □

6. Numerical experiments

The ability of the X-FEM analysis to catch the analytical solution is assessed through the relative energy error, namely:

$$\text{energy error} = \frac{\sqrt{\int_{\Omega_1^h} \epsilon\left(\bar{u}_1 - u_h\right) : A : \epsilon\left(\bar{u}_1 - u_h\right)}}{\sqrt{\int_{\Omega_1} \epsilon\left(u_1\right) : A : \epsilon\left(u_1\right)}}. \tag{67}$$

This is equivalent to the $H^1\left(\Omega_1^h \cup \Omega_2^h\right)$-norm considered in Section 5: as in [19,20], u_h is compared with an extension $\bar{u}$ rather than with u. Comparing thus solutions domainwise, we study in practice the impact of an approximated geometry on the solution over a domain of interest: the matter, as opposed to the holes. This corresponds to the actual engineering concern. The expected convergence rates are given in Table 1.

6.1. Plate with a hole under tension

In this test, tested with an X-FEM formulation in [27], an infinite plate with a central hole is subjected to a uniform traction σ along the x-axis. In plane stress, the analytical solution of the problem, as available in [27], is:

$$\sigma_{xx}(r,\theta) = \sigma\left(1 - \frac{a^2}{r^2}\left[\frac{3}{2}\cos(2\theta) + \cos(4\theta)\right] + \frac{3}{2}\frac{a^4}{r^4}\cos(4\theta)\right) \tag{68}$$

$$\sigma_{yy}(r,\theta) = \sigma\left(-\frac{a^2}{r^2}\left[\frac{1}{2}\cos(2\theta) - \cos(4\theta)\right] - \frac{3}{2}\frac{a^4}{r^4}\cos(4\theta)\right) \tag{69}$$

$$\sigma_{xy}(r,\theta) = \sigma\left(-\frac{a^2}{r^2}\left[\frac{1}{2}\sin(2\theta) + \sin(4\theta)\right] + \frac{3}{2}\frac{a^4}{r^4}\sin(4\theta)\right). \tag{70}$$

In practice, a square plate is considered of length 2 m with a hole radius $a = 0.4$ m. A contour traction is prescribed on its edges, immediately deduced from the analytical stress (see [27,18]). To prevent any rigid-body motion, the displacement is prevented along the x-axis at the middle of the upper and lower edges, and along the y-axis at the middle of the lateral edges (see Fig. 12). The material is isotropic and elastic, with parameters $E = 10^5$ Pa and $\nu = 0.3$.

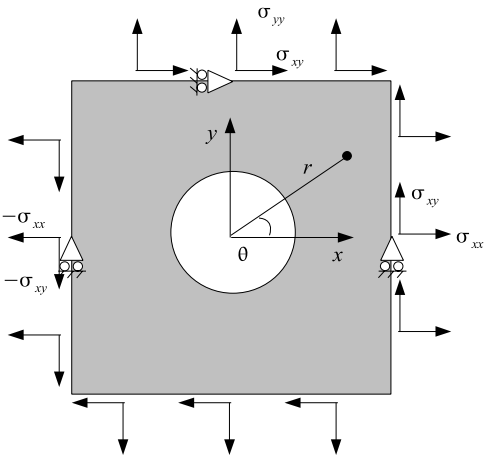

Fig. 12. Numerical test: model and loading.

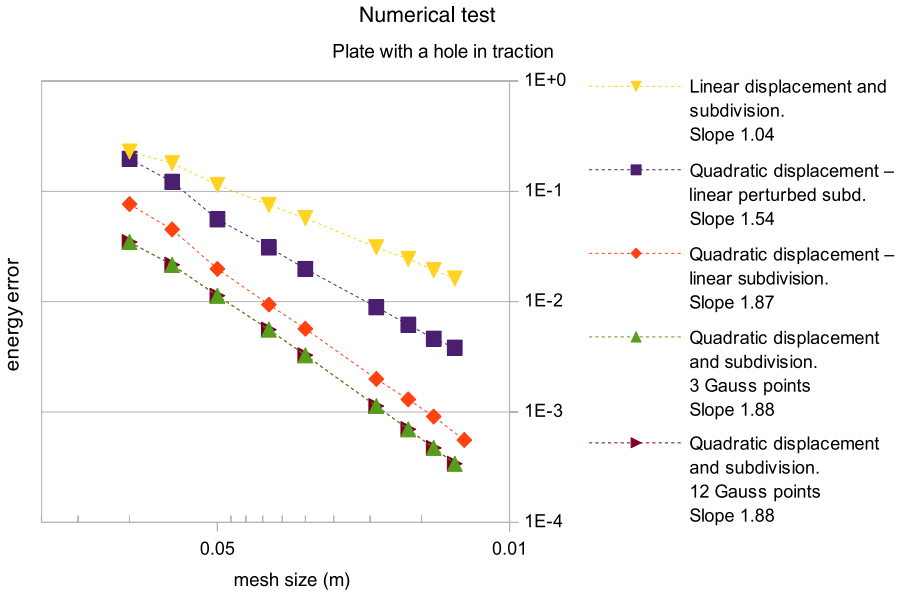

Fig. 13. Numerical results for a problem with a strong discontinuity.

The orders of convergence for P2 or P1 interpolation and subdivision were close to the theoretical values (see Fig. 13). However, and in accordance with the results in [16,17], the case of a P2 displacement with a P1 subdivision yielded a superconvergent rate 1.87, closer to 2 than to the theoretical value 1.5, though values themselves are significantly higher. This superconvergence probably occurs due to symmetry effects related to the circular surface. To highlight this fact, the geometry description is perturbed by a randomly distributed quantity $O\left(h^2\right)$, corresponding to the geometry error determined in Section 4 for a linear subdivision. We then observed a recovered theoretical rate 1.5 (see Fig. 13).

Moreover, several quadrature rules were tested over the subcells, from 3-point to 12-point Gauss schemes. Very little influence could be observed, as can be seen in Fig. 13. Given that 3-point Gauss rule exactly integrates elements of $P_2(\hat{K})$, it seems like an exact integration of elements in $P_2(\hat{K})$ suffices to yield optimal orders of convergence, which is precisely the case in FEM (see [19]).

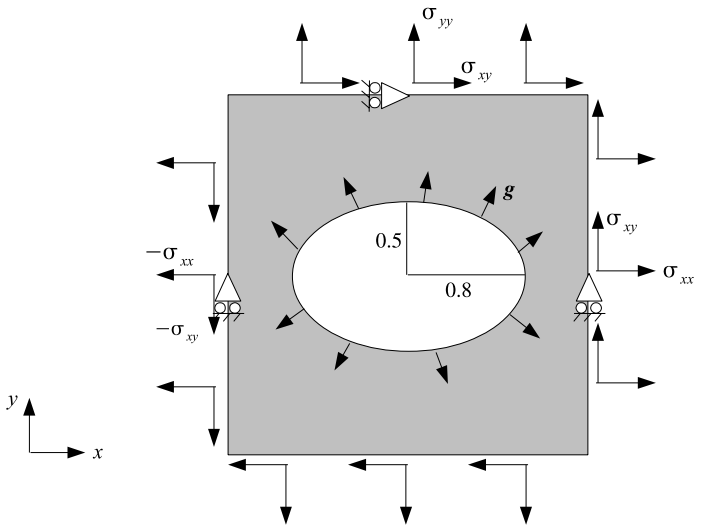

Fig. 14. Plate with an elliptic hole: geometry and loading.

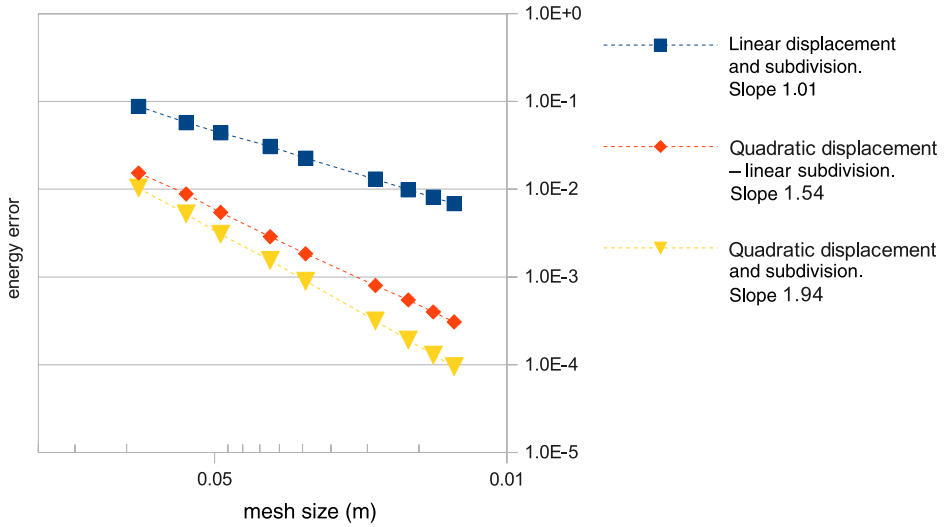

Fig. 15. Plate with an elliptic hole: results.

6.2. Plate with an elliptic hole

This time, an elliptic hole is inserted into the plate (see Fig. 14), which is subjected to surfaces forces $\boldsymbol{g} = \boldsymbol{\sigma} \cdot \boldsymbol{n}$ where $\boldsymbol{\sigma}$ obeys (68)–(70) and $\boldsymbol{n}$ is the normal vector to the ellipse. In this way, the analytical solution (68)–(70) still applies.

The observed convergence rate are close to their predicted values (see Fig. 15), thus ensuring the optimality of the estimates. In particular, the distinction between linear and quadratic subdivision is more obvious, with respective convergence rates 1.54 and 1.94 close to their theoretical values.

6.3. A practical study of problematic cases

Let us now discuss practical aspects, to see if the demonstration shortcomings really induce problems or are just theoretical subtleties. Let us first investigate whether a poor integration scheme actually induces outstanding quadrature errors in badly shaped subcells, that is to say slender or crescent-shaped subcells, according to

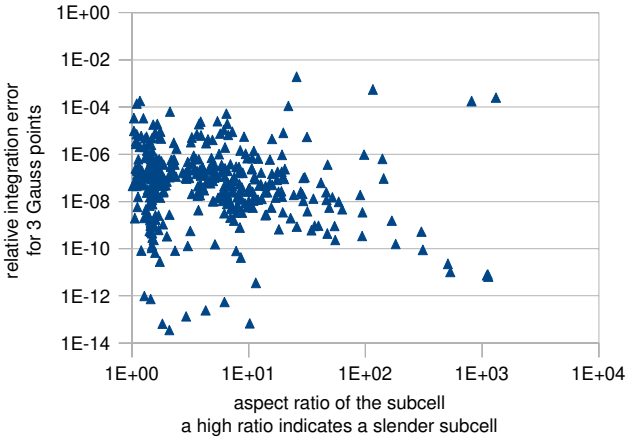

Fig. 16. Quadrature error: crescent-shaped subcells.

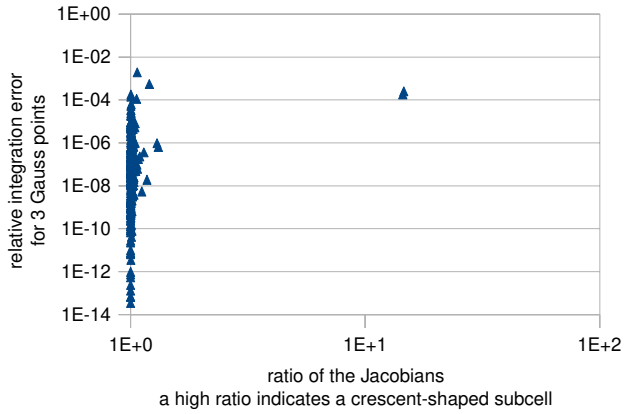

Fig. 17. Quadrature error: slender subcells.

Definition 5.2. We have plotted in Figs. 16 and 17 the local relative integration errors for all curved subcells, respectively with respect to the aspect ratio h_E/ρ_E of the subcell and ratio of the Jacobians $|J_E^{-1}|_{0,\infty,E}|J_E|_{0,\infty,\hat{K}}$: the first is high for a *slender* subcell (Fig. 16) and the other is high for a *crescent-shaped* subcell. Two conclusions emerge from Figs. 16 and 17.

1. The quadrature error in slender subcells appears to be no larger than that of regular subcells, when tested with the rather poor quadrature scheme recommended for the latter. Hence, the quadrature in slender subcells seems to require no particular treatment. The reader is referred to Remark 5.3 for an explanation of the phenomenon.
2. The quadrature error for crescent-shaped subcells appears rather higher than the other values, though there are not enough points to assert it with certainty. For our strategy, there are indeed very few of them, too few to have a significant impact on the error. However, for a subdivision strategy that would involve a lot of crescent-shaped subcells, suboptimal rates may be obtained if the quadrature scheme is not increased, as has been observed in [18].

Secondly, we recall that we have proven convergence properties with respect to the geometry error in Theorem 5.1 excluding the case of lengthways intersected triangles (see Definition 4.2). Denoting N the number of intersected triangles K, let $\Delta E_K = \int_{\Omega_1^h \cap K} \epsilon(\bar{u}_1 - u_h) : A : \epsilon(\bar{u}_1 - u_h)\, d\Omega$, $E_K = \int_{\Omega_1^h \cap K} \epsilon(\bar{u}_1) : A : \epsilon(\bar{u}_1)\, d\Omega$ and $\bar{E} = \sum_{K=1}^{N} E_K/N$. We have plotted in Fig. 18 the local relative energy errors $\Delta E_K/\bar{E}$ for the above problem of a plate with a hole, as a function of the characteristic ratio of the intersection (21), which is high for lengthways intersected triangles. The normalization has been done with the average local energy on tested elements, so as to prevent the spurious effect of higher local interpolation errors on small sections mentioned in Section 5.

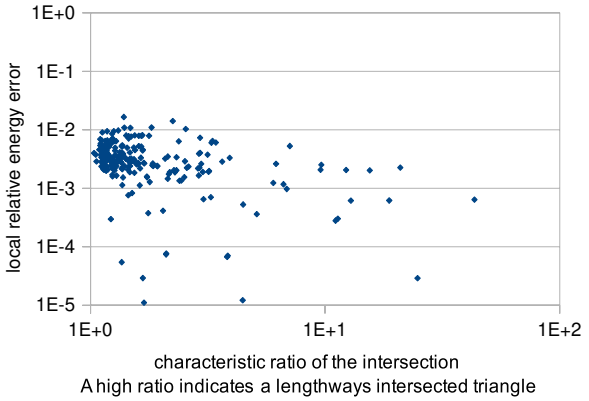

Fig. 18. The effect of lengthways intersected elements: test 1.

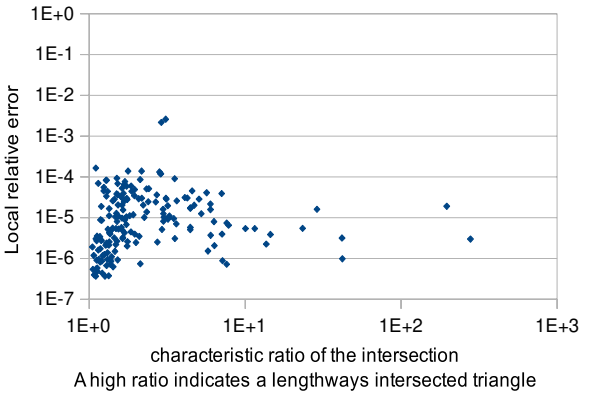

Fig. 19. The effect of lengthways intersected elements: test 2.

In Fig. 19, we have considered another test of a full plate (no hole) under uniaxial tension, whose boundary has been perturbed according to the $O\left(h^2\right)$ error measure determined in Section 4 for linear subdivision. As the exact displacement is spanned by the basis, there is no interpolation in this case, so we have directly plotted the local relative error given by $\Delta E_K / E_K$. Both in Figs. 18 and 19, we see that errors do not increase for lengthways intersected triangles, so this suggests that the exclusion of lengthways intersected triangles from the theoretical estimate is not a practical issue. We propose in Appendix C a proof of convergence for lengthways intersected triangles in a simplified case: this analysis shows that the only problematic case will be detected beforehand by the subdivision process, so that there will be no negative impact over the convergence.

7. Conclusion

The practical conclusion of these special cases of study is that a subdivision with subcells with the same order than the finite-element mesh, used along with the classical related quadrature scheme, is successful to yield optimal orders of convergence. As for the theory, theoretical a-priori error estimates were derived in this paper for the X-FEM method which take into account quadrature effects and the description of the geometry, and can anticipate the convergence rate of a formulation, and predict whether it will be optimal or not. Our estimates hold for linear or quadratic elements, but we believe that the methodology can easily be extended to higher orders.

Acknowledgments

The authors are particularly grateful to Dr Billaud-Friess and Pr Patrick Hild for helping to improve the manuscript and for giving meaningful mathematical advice.

Appendix A. Constructing level-sets from implicit or parametric representation

We need to define regularity properties for the curve Γ to be represented. Here, it is assumed to have a geometric continuity G^k with $k \geq 2$: in general this means that Γ is part of the boundary of an open set Ω of class C^k, which is translated by Eqs. (72)–(74) for an implicit representation, and means that Γ admits a parametrization of class C^k.

Then, we derive level-sets in the upcoming lemma. Note that we always need the assumption of a regular *closed* curve to do so. Hence if Γ is open, it has to be regularly extended beyond its extremities to get a regular level-set. This phenomenon has already been highlighted by Fries [15].

Lemma A.1. *Let Ω be a bounded open set of class C^k with $k \geq 2$, whose boundary is denoted $\partial\Omega$. Then there exists $\delta > 0$ such that the following mapping be a C^{k-1}-diffeomorphism:*

$$\begin{array}{l} \Xi : \partial\Omega \times]-\delta, \delta[\to S_\delta \subset \mathbb{R}^2 \\ (\boldsymbol{x}, t) \to \boldsymbol{x} + t\boldsymbol{n}(\boldsymbol{x}). \end{array} \tag{71}$$

Its inverse will be denoted $\Xi^{-1} : \ y \to (\pi(y), \phi(y))$. $\pi(y)$ is then called the orthogonal projection onto $\partial\Omega$. In the case where Ω is convex, it coincides for points outside D with the classical definition of the orthogonal projection onto a convex set. $\phi(y)$ is our object of interest, it is called the signed distance function to $\partial\Omega$ and used as a definition of the exact level-set.

Proof. By definition of the regularity of a bounded open set, there exists a function $\varphi \in C^k(\mathbb{R}^2)$ such that:

$$\Omega = \{\boldsymbol{x} \in \mathbb{R}^2, \varphi(\boldsymbol{x}) < 0\} \tag{72}$$

$$\partial\Omega = \{\boldsymbol{x} \in \mathbb{R}^2, \varphi(\boldsymbol{x}) = 0\} \tag{73}$$

$$\exists c > 0, \ \forall \boldsymbol{x} \in \partial\Omega, \quad |\nabla\varphi|(\boldsymbol{x}) \geq c. \tag{74}$$

So $\partial\Omega$ is an implicitly defined curve, whose points are all regular. So we may define unit normal and tangent vectors to this curve:

$$\boldsymbol{n}(\varphi) \coloneqq \frac{\nabla\varphi}{|\nabla\varphi|} \tag{75}$$

and:

$$\boldsymbol{t}(\varphi) \coloneqq \mathrm{Rot}_{\frac{-\pi}{2}}(\boldsymbol{n}(\varphi)). \tag{76}$$

With the help of the implicit functions theorem, there is a regular parametrization of $\partial\Omega$ in the vicinity of each of its points. Let $\boldsymbol{x} \in \partial\Omega$, there exists an open portion of the curve containing $\boldsymbol{x}$ which admits a regular parametrization, that we can C^k-equivalently reparametrize with a normal parametrization $s \to f_{\boldsymbol{x}}(s)$. Then, the definition of the directional derivative on the differential manifold $\partial\Omega$ yields for the derivative relative to the first variable:

$$\frac{\partial\Xi}{\partial x} = \boldsymbol{t}(s) + t\frac{d\boldsymbol{n}(s)}{ds} = (1 - t\gamma(s))\,\boldsymbol{t}(s) \tag{77}$$

where we have made use of the Fréchet formula and called the curvature γ.

The derivative relative to the second variable is simply:

$$\frac{\partial\Xi}{\partial t} = \boldsymbol{n}(s). \tag{78}$$

Hence the first derivative $D\Xi$ is:

$$D\Xi = (1 - t\gamma(\varphi))\,\boldsymbol{t}(\varphi) \otimes \boldsymbol{t}(\varphi) + \boldsymbol{n}(\varphi) \otimes \boldsymbol{n}(\varphi) \tag{79}$$

where the curvature is bounded. Indeed, since φ is of class C^2 on a compact set on the first hand, its gradient is bounded away from zero in the other, and $\gamma(\varphi) = \frac{\boldsymbol{t}(\varphi)^T \cdot D^2\varphi \cdot \boldsymbol{t}(\varphi)}{|\nabla\varphi|}$ (see [21]), we may deduce that there exists $R_0 > 0$ such that $|\gamma(\varphi)| < \frac{1}{R_0}$. Let $\boldsymbol{\xi} \in \mathbb{R}^2$, denoting $|\cdot|$ any norm on $\mathbb{R}^2$, we have $|D\Xi(\boldsymbol{\xi})| \geq |\boldsymbol{\xi}|\left(1 - \frac{|t|}{R_0}\right)$. Let us set $\delta < R_0$, then $\inf_\xi \frac{|D\Xi(\boldsymbol{\xi})|}{|\boldsymbol{\xi}|} \geq 1 - \frac{\delta}{R_0} > 0$. Hence $D\Xi$ is invertible, and $|D\Xi^{-1}| \leq \frac{1}{1-\delta/R_0}$.

We have shown that Ξ has a nonzero Jacobian everywhere. Let us prove that it is injective. By contradiction, let $\boldsymbol{x}, \boldsymbol{x}'$ be distinct points on $\partial\Omega$ such that there exists $(t, t') \in]-\delta, \delta[^2$ verifying $\boldsymbol{x} + t\boldsymbol{n}(\boldsymbol{x}) = \boldsymbol{x}' + t'\boldsymbol{n}(\boldsymbol{x}')$. As a consequence $|\boldsymbol{x} - \boldsymbol{x}'| \leq \delta|\boldsymbol{n}(\boldsymbol{x}) - \boldsymbol{n}(\boldsymbol{x}')|$ and since the curvature is bounded $|\boldsymbol{n}(\boldsymbol{x}) - \boldsymbol{n}(\boldsymbol{x}')| \leq R_0^{-1}|(\boldsymbol{x}) - (\boldsymbol{x}')|$, so $|\boldsymbol{x} - \boldsymbol{x}'| \leq \delta/R_0|\boldsymbol{x} - \boldsymbol{x}'|$ which is impossible since $\delta/R_0 < 1$. After the global inversion theorem, we conclude that Ξ is a C^{k-1} diffeomorphism. □

Lemma A.2. *Let Γ be a closed regular simply-connected parametric curve, represented by a parametrization $\boldsymbol{f} : \begin{smallmatrix} I \subset \mathbb{R} \to \mathbb{R}^2 \\ s \to \boldsymbol{f}(s) \end{smallmatrix}$ of class C^k with $k \geq 2$. Then there exists $\delta > 0$ such that the following mapping be a C^{k-1}-diffeomorphism:*

$$\Xi : \begin{matrix} I \times]-\delta, \delta[\to S_\delta \subset \mathbb{R}^2 \\ (s, t) \to \boldsymbol{f}(s) + t\boldsymbol{n}(s). \end{matrix} \tag{80}$$

This lemma is similar to Lemma A.1, but for parametrically-represented curves of geometrical continuity G^k.

Proof. The assumptions on $\boldsymbol{f}$ imply that it is C^k-equivalent to the normal parametrization. Without loss of generality, the parametrization may therefore be considered normal. The curvature is bounded since it is expressed as $\gamma(s) = -\boldsymbol{t}(s)^T \cdot D\boldsymbol{n}(s) \cdot \boldsymbol{t}(s)$ and $\boldsymbol{f}$ is of class C^2. The Jacobian of Ξ is then found to be bounded away from zero proceeding as in Lemma A.1 and the injectivity of Ξ is proven in the same way, knowing that $\boldsymbol{f}(s') = \boldsymbol{f}(s)$ yields $s' = s$ since the curve is simple. □

Remark A.1. Suppose that assumptions of either Lemma A.1 or Lemma A.2 hold. Then the signed distance function is of class C^{k-1}, by definition of a C^{k-1}-diffeomorphism.

Appendix B. Transfinite maps and their errors

Lemma B.1. *Let Γ be a curved interface admitting the normal parametrization in the local basis of Fig. 20 $\begin{cases} I \to \mathbb{R} \\ s \to f(s) = (x(s), y(s)) \end{cases}$. Let $[s_1, s_2] \subset I$ such that $\boldsymbol{f} \in C^{g+1}([s_1, s_2])$. Let $\tilde{E}$ be a transfinite subcell whose boundary matches Γ exactly on $[s_1, s_2]$. Then denoting $\tilde{F}_{\tilde{E}}$ the transfinite map, F_E the corresponding isoparametric map (see Fig. 20) and $R_E := \tilde{F}_{\tilde{E}} - F_E$, we have $\|R_E\|_{g+1,\infty,\hat{K}} \leq Ch^{g+1}|\boldsymbol{f}|_{g+1,\infty,[s_1,s_2]}$ where C is independent of h and $\boldsymbol{f}$.*

Actually, with the notations of Fig. 5, the characteristic size of the subcell is $\hat{\lambda}_M h$, so we have $\|R_E\|_{g+1,\infty,\hat{K}} \leq Ch^{g+1}\hat{\lambda}_M^{g+1}|\boldsymbol{f}|_{g+1,\infty,[s_1,s_2]}$.

Proof. We refer the reader to the Appendix A of [23] for a comprehensive proof in the case $g = 1$. We shall detail the proof in the case where $g = 2$.

Step 1: Introduce an explicit definition of Γ on $[s_1, s_2]$ and show that $h = O\left(|\boldsymbol{x}_3^E - \boldsymbol{x}_1^E|\right)$. Using the appropriate local system of coordinates (see Fig. 20), we observe that $y(s_1) = y(s_2) = 0$. Hence with Rolle's theorem $\exists s_x \in [s_1, s_2]$, $y'(s_x) = 0$. Let us set $h := |s_2 - s_1|$ and $h_0 < |\boldsymbol{f}|_{2,\infty,I}^{-1}$, for $h < h_0$, the Taylor inequality on interval $[s_x, s]$ yields $x'(s)^2 = 1 - y'(s)^2 \geq 1 - (h/h_0)^2 > 0$. So x is C^3 and strictly monotonic on $[s_1, s_2]$, hence it is invertible and the inverse $s : \begin{cases} [0, |\boldsymbol{x}_1^E - \boldsymbol{x}_3^E|] \to [s_1, s_2] \\ x \to s(x) \end{cases}$ is C^3.

Moreover $h \leq \int_{s_1}^{s_2} x'(s)ds + \int_{s_1}^{s_2} |y'(s)|ds \leq |\boldsymbol{x}_3^E - \boldsymbol{x}_1^E| + (h/h_0)\, h$, hence $|\boldsymbol{x}_3^E - \boldsymbol{x}_1^E| \geq (1 - h/h_0)h$. So when the mesh is sufficiently small, h and $|\boldsymbol{x}_3^E - \boldsymbol{x}_1^E|$ are equivalent quantities. From here onward we will then rather work with $h := |\boldsymbol{x}_3^E - \boldsymbol{x}_1^E|$. We may define the part of Γ that the subcell approximates explicitly $\Gamma : y = \nu(x)$ where $\nu : \begin{cases} [0, h] \to \mathbb{R} \\ x \to y(s(x)) \end{cases}$. The regularity assumptions about $\boldsymbol{f}$ and the regularity of s yield $\nu \in C^3([0, h])$.

Step 2: Introduce the polynomial and transfinite maps and prove $|R_E|_{0,\infty,\hat{K}} \leq Ch^3|\boldsymbol{f}|_{3,\infty,[s_1,s_2]}$. Calling $(\hat{\lambda}_i)_{i\in\{1..3\}}$ the reference barycentric coordinates ($\hat{\boldsymbol{x}}(\hat{\lambda}_1, \hat{\lambda}_2)$ and $\hat{\lambda}_3 = 1 - \hat{\lambda}_1 - \hat{\lambda}_2$), and N_{13} the quadratic shape function of the

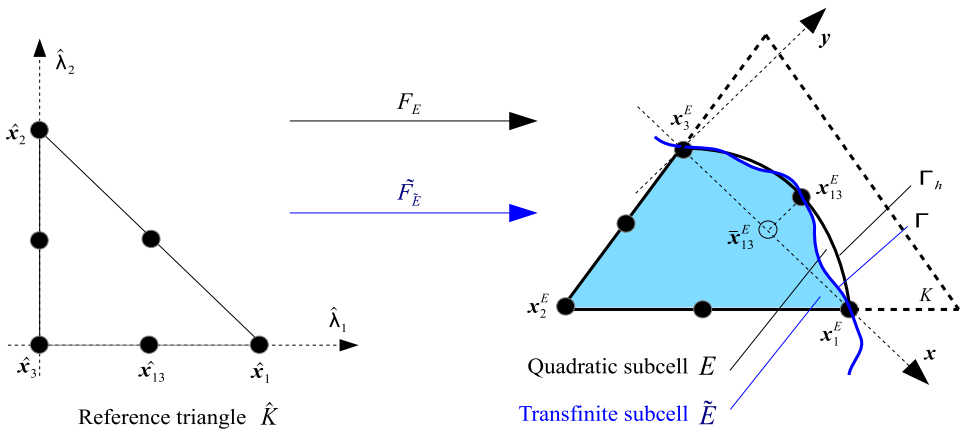

Fig. 20. Classical and transfinite subcells, and local system of coordinates.

node located at $\hat{\boldsymbol{x}}_{13}$, the expressions of the polynomial and transfinite maps are (see the Appendix of [23]):

$$F_E(\hat{\boldsymbol{x}}) = \sum_{i=1}^{3} \hat{\lambda}_i \boldsymbol{x}_i^E + \left(\boldsymbol{x}_{13}^E - \bar{\boldsymbol{x}}_{13}^E\right) N_{13} = \sum_{i=1}^{3} \hat{\lambda}_i \boldsymbol{x}_i^E + 4y \left(\boldsymbol{x}_{13}^E\right) \hat{\lambda}_1 \hat{\lambda}_3 \boldsymbol{y} \tag{81}$$

$$\tilde{F}_{\tilde{E}}(\hat{\boldsymbol{x}}) = \sum_{i=1}^{3} \hat{\lambda}_i \boldsymbol{x}_i^E + \frac{1-\hat{\lambda}_1-\hat{\lambda}_2}{1-\hat{\lambda}_1} \nu(\hat{\lambda}_1 h) \boldsymbol{y}. \tag{82}$$

Then $R_E := F_E - \tilde{F}_{\tilde{E}}$ has the expression $R_E\left(\hat{\boldsymbol{x}}\right) = \frac{\hat{\lambda}_3}{\hat{\lambda}_3+\hat{\lambda}_2} \nu(\hat{\lambda}_1 h) - 4\nu(\frac{h}{2})\hat{\lambda}_1\hat{\lambda}_3$. Let us pose $\hat{\nu}(\hat{\lambda}_1) := \nu(\hat{\lambda}_1 h)$, the error would then take the appropriate form:

$$R_E\left(\hat{\boldsymbol{x}}\right) = \frac{\hat{\lambda}_3}{\hat{\lambda}_2+\hat{\lambda}_3} R_E\left(\hat{\lambda}_1\right) \tag{83}$$

where $R_E(\hat{\lambda}_1) := \hat{\nu}(\hat{\lambda}_1) - 4\hat{\nu}(\frac{1}{2})\hat{\lambda}_1(1-\hat{\lambda}_1)$ is the residual along the lower edge $[\hat{\boldsymbol{x}}_3, \hat{\boldsymbol{x}}_1]$ of the reference triangle in Fig. 20. Hence $|R_E\left(\hat{\boldsymbol{x}}\right)| \leq |R_E(\hat{\lambda}_1)|$ with equality if $\hat{\boldsymbol{x}}$ belongs to that edge. We may then consider this case without loss of generality. Expanding $\hat{\nu}$ to the Taylor series at 0, 1 and 1/2 gives:

$$\begin{aligned}
\hat{\nu}(\hat{\lambda}_1) &= \hat{\lambda}_1 \hat{\nu}'(0) + \hat{\lambda}_1^2 \frac{\hat{\nu}''(0)}{2} + R_2(0;\hat{\lambda}_1) \\
&= (\hat{\lambda}_1 - 1)\hat{\nu}'(1) + (\hat{\lambda}_1 - 1)^2 \frac{\hat{\nu}''(1)}{2} + R_2(1;\hat{\lambda}_1) \\
&= \hat{\nu}\left(\frac{1}{2}\right) + \left(\hat{\lambda}_1 - \frac{1}{2}\right)\hat{\nu}'\left(\frac{1}{2}\right) + \left(\hat{\lambda}_1 - \frac{1}{2}\right)^2 \frac{\hat{\nu}''\left(\frac{1}{2}\right)}{2} + R_2\left(\frac{1}{2};\hat{\lambda}_1\right)
\end{aligned} \tag{84}$$

where the Laplace residual has been noted $R_k(a;b) := \int_a^b \frac{\hat{\nu}^{(3)}(t)}{k!}(b-t)^k\, dt$ for $k \in \{0,1,2\}$.

We may then multiply each of the above Taylor series with its corresponding shape function along the segment: the series at 0, 1 and 1/2 are respectively multiplied by $N_3(\hat{\lambda}_1) = (1-2\hat{\lambda}_1)(1-\hat{\lambda}_1)$, $N_1(\hat{\lambda}_1) = \hat{\lambda}_1(2\hat{\lambda}_1 - 1)$ and $N_{13}(\hat{\lambda}_1) = 4\hat{\lambda}_1(1-\hat{\lambda}_1)$. Owing to the fact that $N_1(\hat{\lambda}_1) + N_{13}(\hat{\lambda}_1) + N_3(\hat{\lambda}_1) = 1$, the addition yields:

$$\begin{aligned}
\frac{R_E(\hat{\lambda}_1)}{\hat{\lambda}_1\left(1-\hat{\lambda}_1\right)\left(1-2\hat{\lambda}_1\right)} &= \left[\hat{\nu}'(0) + \hat{\nu}'(1) - 2\hat{\nu}'(1/2)\right] \\
&\quad + \frac{1}{2}\left[\hat{\lambda}_1\hat{\nu}''(0) + (\hat{\lambda}_1 - 1)\hat{\nu}''(1) + (1-2\hat{\lambda}_1)\hat{\nu}''(1/2)\right] \\
&\quad + \frac{R_2(0;\hat{\lambda}_1)}{\hat{\lambda}_1} - \frac{R_2(1;\hat{\lambda}_1)}{1-\hat{\lambda}_1} + 4\frac{R_2(1/2;\hat{\lambda}_1)}{1-2\hat{\lambda}_1}.
\end{aligned} \tag{85}$$

Further expansion into the Taylor series of $\hat{\nu}'(0)$, $\hat{\nu}'(1)$, $\hat{\nu}''(0)$ and $\hat{\nu}''(1)$ around $1/2$ allows to cancel out first and second order terms in the above expression:

$$\hat{\nu}'(0) + \hat{\nu}'(1) - 2\hat{\nu}'(1/2) = R_1(1/2;0) + R_1(1/2;1) \tag{86}$$

$$\hat{\lambda}_1\hat{\nu}''(0) + (\hat{\lambda}_1 - 1)\hat{\nu}''(1) + (1-2\hat{\lambda}_1)\hat{\nu}''\left(\frac{1}{2}\right) = \hat{\lambda}_1 R_0\left(\frac{1}{2};0\right) + (\hat{\lambda}_1 - 1)R_0\left(\frac{1}{2};1\right). \tag{87}$$

Hence:

$$\begin{aligned}\frac{R_E(\hat{\lambda}_1)}{\hat{\lambda}_1\left(1-\hat{\lambda}_1\right)\left(1-2\hat{\lambda}_1\right)} &= R_1(1/2;0) + R_1(1/2;1) + \frac{1}{2}\left[\hat{\lambda}_1 R_0(1/2;0) + (\hat{\lambda}_1 - 1)R_0(1/2;1)\right] \\ &\quad + \frac{R_2(0;\hat{\lambda}_1)}{\hat{\lambda}_1} - \frac{R_2(1;\hat{\lambda}_1)}{1-\hat{\lambda}_1} + 4\frac{R_2(1/2;\hat{\lambda}_1)}{1-2\hat{\lambda}_1}.\end{aligned} \tag{88}$$

From this expression it is obvious that:

$$|R_E|_{0,\infty,K} \leq C|\hat{\nu}|_{3,\infty,[0,1]} \leq Ch^3|\nu|_{3,\infty,[0,h]} \leq Ch^3|\boldsymbol{f}|_{3,\infty,[s_1,s_2]}. \tag{89}$$

Step 3: Prove the same properties for the derivatives with respect to $\hat{\boldsymbol{x}}(\hat{\lambda}_1, \hat{\lambda}_2)$.
Combining (88) with (83), we have:

$$\begin{aligned}\frac{R_E(\hat{\boldsymbol{x}})}{\hat{\lambda}_1\hat{\lambda}_3\left(1-2\hat{\lambda}_1\right)} &= R_1(1/2;0) + R_1(1/2;1) + \frac{1}{2}\left[\hat{\lambda}_1 R_0(1/2;0) + (\hat{\lambda}_1 - 1)R_0(1/2;1)\right] \\ &\quad + \frac{R_2(0;\hat{\lambda}_1)}{\hat{\lambda}_1} - \frac{R_2(1;\hat{\lambda}_1)}{1-\hat{\lambda}_1} + 4\frac{R_2(1/2;\hat{\lambda}_1)}{1-2\hat{\lambda}_1}.\end{aligned} \tag{90}$$

Let $a \in [0,1]$. We have $\frac{\partial R_0(a;\hat{\lambda}_1)}{\partial\hat{\lambda}_1} = \hat{\nu}^{(3)}(\hat{\lambda}_1)$. Let $l \in \{1,2\}$, it comes $\frac{\partial R_l(a;\hat{\lambda}_1)}{\partial\hat{\lambda}_1} = R_{l-1}(a;\hat{\lambda}_1)$. Hence, for $m \in \{0..3\}$, a straightforward recursion yields $\left|\frac{\partial^m R_2(a;\hat{\lambda}_1)}{\partial\hat{\lambda}_1^m}\right| \leq |\hat{\nu}|_{3,\infty,[0,1]}|\hat{\lambda}_1 - a|^{3-m}$. The only term of (90) that could be problematic to prove the result is $\frac{\hat{\lambda}_3 R_2(1;\hat{\lambda}_1)}{1-\hat{\lambda}_1}$. Its k-order derivative with respect to $\hat{\boldsymbol{x}}$, $k \in \{0..3\}$, involves terms of the form $R_{k;m,l} := \frac{1}{(1-\hat{\lambda}_1)^{l+1}}\left(\frac{\partial^m(\hat{\lambda}_3)}{\partial\hat{\lambda}_i^m}\frac{\partial^{k-m-l}R_2(1;\hat{\lambda}_1)}{\partial\hat{\lambda}_1^{k-m-l}}\right)$ where $m \in \{0,1\}$, $i \in \{1,2\}$ and l is an integer verifying $m + l \leq k$. In case $m = 0$, we have:

$$|R_{k;m,l}| \leq \frac{\hat{\lambda}_3}{1-\hat{\lambda}_1}\frac{\left|D^{k-l}R_2(1,\hat{\lambda}_1)\right|}{(1-\hat{\lambda}_1)^l} \leq |\hat{\nu}|_{3,\infty,[0,1]}|1-\hat{\lambda}_1|^{3-k}. \tag{91}$$

Else, if $m = 1$ then $|R_{k;m,l}| \leq \frac{\left|D^{k-(l+1)}R_2(1,\hat{\lambda}_1)\right|}{\left|1-\hat{\lambda}_1\right|^{l+1}} \leq |\hat{\nu}|_{3,\infty,[0,1]}|1-\hat{\lambda}_1|^{3-k}$, so we get to bound all derivatives of R_E with $|\hat{\nu}|_{3,\infty,[0,1]}$, which given (89) yields the results that we intended to prove $\|R_E\|_{3,\infty,K} \leq Ch^3|\boldsymbol{f}|_{3,\infty,[s_1,s_2]}$. □

Appendix C. Elements of proof for lengthways intersected elements

In this appendix, we derive an estimate of the error due to the change in domain in the case of lengthways intersected triangle, under the simplifying assumptions that (to alleviate expressions):

- the interpolation is linear,
- the subdivision is linear,
- there is no "source term": $f = 0$,
- the conductivity is isotropic and uniform: $\boldsymbol{A} = \mathbf{1}$.

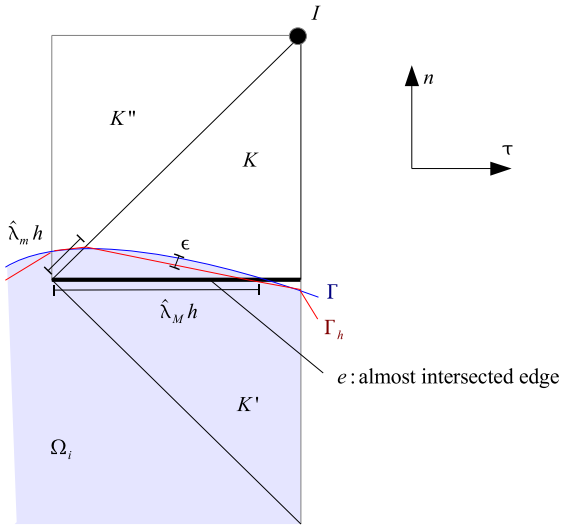

Fig. 21. Lengthways intersected triangle.

To this aim, we would like to refine estimate (c) in (26) by getting rid of the superior bound in the consistency estimates $\sup_{w_h \in V_h} \frac{|\check{a}_h(\bar{u}, w_h) - a(u, \bar{w}_h)|}{\|w_h\|_{1,\Omega_1^h \cup \Omega_2^h}}$. Considering again the proof of Proposition 5.1, and the proof of Theorem 4.1.1 in [19], it can be seen that it actually suffices to consider $w_h = u_h - \Pi_h u$. Abiding by the same principle, Strang and Fix [20] also proposed an analysis of the error due to the change of domain by introducing $\check{u}_h$ that would be the solution over the discrete space if the operators were computed on the exact domain:

$$\forall v_h \in V_h, \quad a\left(\check{u}_h, v_h\right) = 0. \tag{92}$$

The authors [20, Section 4.4] would then study $E := \|u_h - \check{u}_h\|_{1,\Omega_1^h \cup \Omega_2^h}$ as the consistency error and come across the estimates:

$$\begin{aligned} E^2 &\leq C \left|a_h\left(u - \check{u}_h, u_h - \check{u}_h\right)\right| + \left|\check{a}_h\left(\bar{u}, u_h - \check{u}_h\right) - a\left(u, \overline{u_h - \check{u}_h}\right)\right| \\ &\leq C h^p E + \epsilon^{1/2} |u_h - \check{u}_h|_{1,S_\epsilon}. \end{aligned} \tag{93}$$

We shall adopt the same paradigm and look for an estimation of the second term. As we have seen in (62), in a lengthways intersected element K (see Fig. 21), the Berger lemma would only give:

$$|u_h - \check{u}_h|^2_{1,S_\epsilon \cap K \cap \Omega_i^h} \leq C \frac{\hat{\lambda}_M}{\hat{\lambda}_m} \frac{\epsilon}{h} |u_h - \check{u}_h|^2_{1,K \cap \Omega_i^h}. \tag{94}$$

So now we aim at finding a better approximation for $|u_h - \check{u}_h|^2_{1,K\cap\Omega_i^h}$ that would remove the $\frac{\hat{\lambda}_M}{\hat{\lambda}_m}$ factor. The gradient is split into a tangential and a normal part to the almost coincident edge e, according to the notations of Fig. 21:

$$\nabla\left(u_h - \check{u}_h\right) = \nabla_\tau\left(u_h - \check{u}_h\right) + \nabla_n\left(u_h - \check{u}_h\right). \tag{95}$$

Given that the gradients are constant over K since the interpolation is linear and that $\text{meas}\left(K \cap \Omega_i^h\right) \leq \hat{\lambda}_m h \text{meas}\left(e \cap \Omega_i^h\right)$ (see Fig. 21), integrating over $K \cap \Omega_i^h$ yields:

$$|u_h - \check{u}_h|^2_{1,K\cap\Omega_i^h} \leq \hat{\lambda}_m h |\nabla_\tau\left(u_h - \check{u}_h\right)|^2_{0,e\cap\Omega_i^h} + |\nabla_n\left(u_h - \check{u}_h\right)|^2_{0,K\cap\Omega_i^h}. \tag{96}$$

We denote K' the adjacent element to K such that $K' \cap K = e$ (see Fig. 21). Element K' obviously verifies $\frac{\text{meas}(K' \cap \Omega_i^h)}{\text{meas}(K')} \geq c$, so that $\text{meas}\left(e \cap \Omega_i^h\right) \leq C \frac{\text{meas}(K')}{h} \leq C \frac{\text{meas}(K' \cap \Omega_i^h)}{h}$. Still keeping in mind that gradients are

constant, we have then:

$$|\nabla_\tau \left(u_h - \check{u}_h\right)|^2_{0,e\cap\Omega_i^h} \leq \frac{C}{h}|\nabla_\tau \left(u_h - \check{u}_h\right)|^2_{0,K'\cap\Omega_i^h}. \tag{97}$$

As for the second term, the discrete translation of the free surface boundary condition makes $\nabla\check{u}_h$ nearly orthogonal to the normal of Γ_h, itself being a close direction to $\boldsymbol{n}_K$ since the element is lengthways intersected. To give it a mathematical translation, we write the weak formulation of the problem:

$$\int_{\Omega_i} \nabla\check{u}_h \cdot \nabla v_h d\Omega = 0. \tag{98}$$

We then choose as a test function the shape function of the opposite node I to the almost coincident edge. In Fig. 21, we would take $v_h = N_I$ for instance. Calling K'' the element belonging to the support of I along with K, it holds:

$$\int_{K\cap\Omega_i} \nabla\check{u}_h \cdot \nabla N_I d\Gamma = -\int_{K''\cap\Omega_i} \nabla\check{u}_h \cdot \nabla N_I d\Gamma. \tag{99}$$

By the same token, we have:

$$\int_{K\cap\Omega_i^h} \nabla u_h \cdot \nabla N_I d\Gamma = -\int_{K''\cap\Omega_i^h} \nabla u_h \cdot \nabla N_I d\Gamma. \tag{100}$$

Since $\nabla N_I|_K$ is directed toward $\boldsymbol{n}_K$, it holds $\nabla N_I|_K = \frac{C}{h}\boldsymbol{n}_K$. Given that ∇u_h and $\nabla\check{u}_h$ are constant elementwise, it may be deduced from (99) that $\nabla\check{u}_h|_K \cdot \boldsymbol{n}_K = -\frac{\text{meas}\left(\Omega_i\cap K''\right)}{\text{meas}(\Omega_i\cap K)}\nabla\check{u}_h|_{K''} \cdot \boldsymbol{n}_{K''}$ and from (100) that $\nabla u_h|_K \cdot \boldsymbol{n}_K = -\frac{\text{meas}\left(\Omega_i^h\cap K''\right)}{\text{meas}\left(\Omega_i^h\cap K\right)}\nabla u_h|_{K''} \cdot \boldsymbol{n}_{K''}$. Subtracting these expressions yields:

$$\begin{aligned}\left|\nabla \left(u_h - \check{u}_h\right) \cdot \boldsymbol{n}_K\right|_K \leq\ & C\frac{\text{meas}\left(\Omega_i^h \cap K''\right)}{\text{meas}\left(\Omega_i^h \cap K\right)}\left|\nabla \left(u_h - \check{u}_h\right)\right|_{K''} \\ & + C\left|\frac{\text{meas}\left(\Omega_i \cap K''\right)}{\text{meas}\left(\Omega_i \cap K\right)} - \frac{\text{meas}\left(\Omega_i^h \cap K''\right)}{\text{meas}\left(\Omega_i^h \cap K\right)}\right|\left|\nabla\check{u}_h\right|_{K''}.\end{aligned} \tag{101}$$

As $\text{meas}\left(\Omega_i^h \cap K''\right) \sim \hat{\lambda}_m^2 h^2$ and $\text{meas}\left(\Omega_i^h \cap K\right) \sim \hat{\lambda}_m\hat{\lambda}_M h^2$, it holds:

$$\frac{\text{meas}\left(\Omega_i^h \cap K''\right)}{\text{meas}\left(\Omega_i^h \cap K\right)} \leq C\frac{\hat{\lambda}_m}{\hat{\lambda}_M}. \tag{102}$$

Moreover, we may decompose:

$$\begin{aligned}\frac{\text{meas}\left(\Omega_i^h \cap K''\right)}{\text{meas}\left(\Omega_i^h \cap K\right)} - \frac{\text{meas}\left(\Omega_i \cap K''\right)}{\text{meas}\left(\Omega_i \cap K\right)} =\ & \frac{\text{meas}\left(\Omega_i^h \cap K''\right) - \text{meas}\left(\Omega_i \cap K''\right)}{\text{meas}\left(\Omega_i^h \cap K\right)} \\ & - \frac{\text{meas}\left(\Omega_i \cap K''\right)}{\text{meas}\left(\Omega_i^h \cap K\right)} \\ & \times \frac{\text{meas}\left(\Omega_i^h \cap K\right) - \text{meas}\left(\Omega_i \cap K\right)}{\text{meas}\left(\Omega_i \cap K\right)}.\end{aligned} \tag{103}$$

We have $|\text{meas}\left(\Omega_i^h \cap K''\right) - \text{meas}\left(\Omega_i \cap K''\right)| \leq \hat{\lambda}_m^2\epsilon h$. The gray area in Fig. 22 may be estimated by $|\text{meas}\left(\Omega_i^h \cap K\right) - \text{meas}\left(\Omega_i \cap K\right)| \leq \hat{\lambda}_M^2\epsilon h$, from which we immediately deduce $\text{meas}\left(\Omega_i \cap K\right) \geq \hat{\lambda}_M h\Big(\hat{\lambda}_m h - \hat{\lambda}_M\epsilon\Big)$. Note that if $\hat{\lambda}_M\epsilon \geq \hat{\lambda}_m h$ then the edge is intersected twice, as represented in Fig. 22(b). In our program, this configuration is detected by the subdivision process and an error is issued since it cannot be handled. So we will

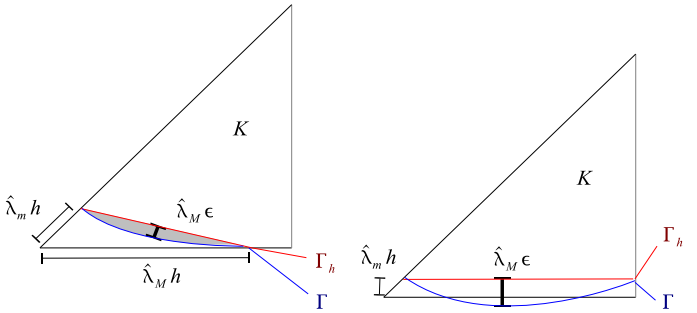

(a) Accepted configuration. (b) Rejected configuration.

Fig. 22. Lengthways intersected triangles.

assume from now on that $\hat{\lambda}_M \epsilon < \hat{\lambda}_m h$. With these estimates and (102), (103) gives:

$$\left| \frac{\text{meas}\left(\Omega_i^h \cap K''\right)}{\text{meas}\left(\Omega_i^h \cap K\right)} - \frac{\text{meas}\left(\Omega_i \cap K''\right)}{\text{meas}\left(\Omega_i \cap K\right)} \right| \leq \frac{\hat{\lambda}_m}{\hat{\lambda}_M} \frac{\epsilon}{h} \left(1 + \frac{C}{\hat{\lambda}_m / \hat{\lambda}_M - \epsilon / h} \right)$$
$$\leq C \frac{\epsilon}{h} \left(1 - \frac{\hat{\lambda}_M}{\hat{\lambda}_m} \frac{\epsilon}{h} \right)^{-1}. \tag{104}$$

Since the gradients are constant by elements, recalling the areas of meas $\left(\Omega_i^h \cap K''\right)$ and meas $\left(\Omega_i^h \cap K\right)$, given (102) and (104), and assuming that $\nabla \check{u}_h$ is bounded we have:

$$\int_{K \cap \Omega_i^h} |\nabla_n \left(u_h - \check{u}_h\right)|^2 d\Omega \leq C \left(\frac{\hat{\lambda}_m}{\hat{\lambda}_M} \int_{K'' \cap \Omega_i^h} |\nabla \left(u_h - \check{u}_h\right)|^2 + \epsilon^2 \hat{\lambda}_m \hat{\lambda}_M \left(1 - \frac{\hat{\lambda}_M}{\hat{\lambda}_m} \frac{\epsilon}{h} \right)^{-2} \right). \tag{105}$$

Combining the results of (105) and (97) in (96), reporting in (94) yields:

$$|u_h - \check{u}_h|^2_{1, K \cap S_\epsilon \cap \Omega_i^h} \leq C \frac{\epsilon}{h} \left(|u_h - \check{u}_h|^2_{1, K' \cap \Omega_i^h} + |u_h - \check{u}_h|^2_{1, K'' \cap \Omega_i^h} \right) + C \frac{\epsilon^3}{h} \hat{\lambda}_M^2 \left(1 - \frac{\hat{\lambda}_M}{\hat{\lambda}_m} \frac{\epsilon}{h} \right)^{-2}. \tag{106}$$

Summing (106) over all lengthways intersected triangles (there are at most $\frac{\text{meas}(\Gamma)}{h}$ of them) yields:

$$|u_h - \check{u}_h|^2_{1, S_\epsilon} \leq C \frac{\epsilon}{h} E^2 + C \frac{\epsilon^3}{h^2} \hat{\lambda}_M^2 \left(1 - \frac{\hat{\lambda}_M}{\hat{\lambda}_m} \frac{\epsilon}{h} \right)^{-2}. \tag{107}$$

Reporting the expression in (93), we have:

$$E^2 - CE \left(h^p + \epsilon h^{-1/2} \right) - C \left(\epsilon h^{-1/2} \right)^2 \left(1 - \frac{\hat{\lambda}_M}{\hat{\lambda}_m} \frac{\epsilon}{h} \right)^{-1} \leq 0. \tag{108}$$

Hence E lies between the roots of this second-order polynomial, so giving a superior bound to the abs-value of the roots, we conclude about the consistency error:

$$E \leq C h^p + C \epsilon h^{-1/2} \left[\left(1 - \frac{\hat{\lambda}_M}{\hat{\lambda}_m} \frac{\epsilon}{h} \right)^{-1/2} + 1 \right]. \tag{109}$$

To conclude about this proof, for lengthways intersected triangles, similar error estimates than Theorem 5.1 may still be derived. If the intersection is convex, as in Fig. 21, the estimate cannot be degenerated. On the contrary, it

can if it is too concave, as in Fig. 22(b), but in such cases the subdivision algorithm alerts us before the estimates get critical.

Notations guide

The symbols are listed following their order of appearance. Note that superscript $\bar{}$ generally indicates an extension (to a larger domain than the original domain of definition for example), superscript $\tilde{}$ indicates quantities defined over a so-called transfinite element (an element with an analytical map, conforming to the exact interface), superscript $\hat{}$ refers to quantities defined over the reference space.

Part 2

Ω full body
Γ interface or crack
$\partial\Omega$ boundary of Ω
Γ_u part of the boundary with a prescribed displacement (Dirichlet boundary conditions)
Γ_g part of the boundary with a prescribed force distribution (Neumann boundary conditions)
i side relative to the interface
Ω_i part of the body on side i
$\boldsymbol{f}$ volume forces
$\boldsymbol{A}$ tensor of elasticity
$\boldsymbol{\sigma}$ Cauchy stress tensor
$\boldsymbol{n}_i$ outward normal vector to Ω_i
$\boldsymbol{u}$ displacement field
$\boldsymbol{u}_i$ restriction of the field $\boldsymbol{u}$ on the side i
$W^{m,p}(\Omega)$ Sobolev space of functions whose derivative up to order m lies in $L^p(\Omega)$
$H^m(\Omega) := W^{m,2}(\Omega)$
$\boldsymbol{x} = (x_1, x_2)$ Cartesian coordinates in $\mathbb{R}^2$
$|\boldsymbol{x}|$ any norm on the finite-dimensional space $\boldsymbol{x}$ belongs to
D derivation operator (e.g. if $\boldsymbol{u}$ is a vector, $D\boldsymbol{u}$ is its Jacobian matrix)
$D^m := \underbrace{D \circ \cdots \circ D}_{m \text{ times}}$ (e.g. if u is scalar, D^2u is its Hessian matrix)
$\nabla : \nabla u$ is the gradient of u, $\nabla \cdot u$ is the divergence of u
$\frac{\partial u}{\partial x_i}$ derivative of u with respect to the i
$\alpha = (\alpha_1, \alpha_2) \in \mathbb{R}^2$ multi-index
$|\alpha| = \alpha_1 + \alpha_2$ size of the multi-index
$\partial^\alpha v := \frac{\partial^{|\alpha|} v}{\partial x_1^{\alpha_1} \partial x_2^{\alpha_2}}$
$|v|_{m,p,\Omega} := \left(\sum_{|\alpha|=m} \int_\Omega |\partial^\alpha v|^p dx \right)^{1/p}$ semi-norm in $W^{m,p}(\Omega)$
$|v|_{m,\infty,\Omega} := \max_{|\alpha|=m} \sup_\Omega |\partial^\alpha v|$ semi-norm in $W^{m,\infty}(\Omega)$
$\|v\|_{m,p,\Omega} := \left(\sum_{|\alpha|\leq m} \int_\Omega |\partial^\alpha v|^p dx \right)^{1/p}$ norm in $W^{m,p}(\Omega)$ or $\|v\|_{m,\infty,\Omega} := \max_{|\alpha|\leq m} \sup_\Omega |\partial^\alpha v|$
$\|v\|_{m,\Omega} := \|v\|_{m,2,\Omega}$
$\|v\|^2_{m,\Omega_1\cup\Omega_2} := \|v\|^2_{m,\Omega_1} + \|v\|^2_{m,\Omega_2}$
C generic non-negative constant
c generic strictly positive constant
V subspace of $H^1(\Omega_1) \times H^1(\Omega_2)$ of functions respecting the Dirichlet boundary conditions
$a \in \mathcal{L}(V \times V; \mathbb{R})$ stiffness bilinear form
$b \in \mathcal{L}(V; \mathbb{R})$ external force linear form
V_h approximation space for V.

Part 3

$\mathcal{T}_h$ affine triangulation of M
K parent element
h_K external radius of an element
ρ_K internal radius of an element
h characteristic mesh size (maximal external radius)
g order of representation of the geometry
ϕ exact level-set function
ϕ_h interpolated level-set function
Γ_ϕ iso-zero of the interpolated level-set
Γ_h approximation of Γ
Ω_i^h approximation of Ω_i
$p \in \{1, 2\}$ order of the interpolation
N_i shape function of order p associated with node i
$\mathcal{N}_h$ nodes of $\mathcal{T}_h$
$\mathcal{E}_h$ cut elements
$\mathcal{K}_h$ enriched nodes
H Heaviside-like function.

Part 4 and appendices

δ semi-width of the strip in which ϕ is defined
S_δ strip of width 2δ centered on Γ
Ξ map whose inverse defines the level-set function
φ function implicitly defining Γ
$\boldsymbol{t}$ tangent vector to a curve
γ curvature
s curvilinear abscissa
R_0 minimal radius of curvature
$\boldsymbol{f}$ normal parametrization of Γ
$\boldsymbol{f}_\phi$ normal parametrization of Γ_ϕ
I definition segment for the parametrization
I_p standard nodal interpolation operator
$P_k(K)$ space of polynomials of total order k on K
δ' semi-width of the strip in which ϕ_h is defined
h_0 upper bound for the mesh size
ϵ resolution of the interface
$\tilde{E}$ transfinite subcell
$\hat{K}$ reference triangle
F_E transformation mapping $\hat{K}$ onto E
$\tilde{F}_{\tilde{E}}$ transfinite transformation mapping $\hat{K}$ onto $\tilde{E}$
R_E residual $\tilde{F}_{\tilde{E}} - F_E$
(x, y) position in the local system of coordinates
$\hat{\boldsymbol{x}}_l$ coordinate of the lth node of the reference element
$\boldsymbol{x}_l^E \coloneqq F_E\left(\hat{\boldsymbol{x}}_l\right)$
ν local explicit definition of Γ on a subcell
$(\hat{\lambda}_i)_{i\in\{1..3\}}$ barycentric coordinates
$\hat{\nu}$ scaled local explicit definition of Γ on a subcell
$R_k(a; b) \coloneqq \int_a^b \frac{\hat{\nu}^{(3)}(t)}{k!}(b-t)^k\, dt$ Laplace residual

$\hat{\lambda}_M$ 1D reference coordinate of the farthest intersection point
$\hat{\lambda}_m$ 1D reference coordinate of the closest intersection point
κ generic tolerance for close intersections.

Part 5

$\bar{\Omega}_i$ domain containing all discretizations
Ω_i^h for a given fixed mesh size
$\bar{u}_i : H^{p+1}$ stable extension of u_i to $\bar{\Omega}_i$
$\bar{u}$ function over $\Omega_1^h \cup \Omega_2^h$ defined by $\bar{u}_i$ over Ω_i^h
E integration subcell
$\left(\hat{w}_l\right)_{l=1..L}$ integration weights
$(\hat{\boldsymbol{b}}_l)_{l=1..L}$ integration points locations
DF_E Jacobian matrix of F_E
$J_E \coloneqq \det(DF_E)$ of inverse J_E^{-1}
$w_{l,E}$ integration weights in the physical space
$\boldsymbol{b}_{l,E}$ integration points location in the physical space
V_h interpolation space for the displacement
a_h discrete bilinear form (approximated domains and quadrature scheme)
l_h discrete linear form (approximated domains and quadrature scheme)
$\breve{a}_h$ intermediate bilinear form (approximated domains and exact integration)
$\breve{l}_h$ intermediate linear form (approximated domains and exact integration)
p, p' elements of $P_2(K)$
$\hat{p} \coloneqq p \circ F_K$ pullback onto the reference parent element of p
$\hat{E} \coloneqq F_K^{-1}(E)$ pullback onto the reference element of a subcell
Π_h X-FEM (discontinuous) interpolation operator onto V_h
a_l classical degree of freedom
b_l enriched degree of freedom
$\hat{\Delta}(.)$ quadrature error over the reference triangle
$\Delta_E(.)$ quadrature error over a subcell
i', j' directions of derivation in the reference space
$\hat{a}$ pullback of A_{ij} onto the reference space (indices are dropped to alleviate notations)
$\bar{w}_h^i$ natural polynomial extension to K of the polynomial function w_h^i defined on $K \cap \Omega_i^h$
$\bar{w}_h$ defined by $\bar{w}_h^i$ on each Ω_i
e almost coincident edge to a lengthways intersected triangle
K' adjacent triangle to a lengthways intersected triangle through its almost coincident edge
$\hat{\bar{w}}_h^i \coloneqq \bar{w}_h^i \circ F_K$.

References

[1] N. Moës, J. Dolbow, T. Belytschko, A finite element method for crack growth without remeshing, Internat. J. Numer. Methods Engrg. 46 (1999) 135–150.
[2] A. Paluszny, R. Zimmerman, Numerical simulation of multiple fracture propagation using arbitrary meshes, Comput. Methods Appl. Mech. Engrg. 200 (2011) 953–966.
[3] A. Tabiei, J. Wu, Development of the DYNA3D simulation code with automated fracture procedure for brick elements, Internat. J. Numer. Methods Engrg. 57 (2003) 1979–2006.
[4] G. Dhondt, A new automatic hexaedral mesher based on cutting, Internat. J. Numer. Methods Engrg. 50 (2011) 1979–2006.
[5] J.M. Melenk, I. Babuška, The partition of unity finite element method: basic theory and applications, Comput. Methods Appl. Mech. Engrg. 39 (1996) 289–314.

[6] F.L. Stazi, E. Budyn, J. Chessa, T. Belytschko, An extended finite elements method with higher order elements for curved cracks, Comput. Mech. 31 (2003) 38–48.
[7] J. Chessa, H. Wang, T. Belytschko, On the construction of blending elements for local partition of unity enriched finite elements, Internat. J. Numer. Methods Engrg. 57 (2003) 1015–1038.
[8] G. Zi, T. Belytschko, New crack tip elements for XFEM and applications to cohesive cracks, Internat. J. Numer. Methods Engrg. 57 (2003) 2221–2240.
[9] P. Laborde, J. Pommier, Y. Renard, M. Salaun, High-order extended finite element method for cracked domains, Internat. J. Numer. Methods Engrg. 64 (2005) 354–381.
[10] E. Chahine, P. Laborde, Y. Renard, Crack tip enrichment in the XFEM method using a cut-off function, Internat. J. Numer. Methods Engrg. 75 (2008) 629–646.
[11] N. Chevaugeon, N. Moes, H. Minnebo, Improved crack-tip enrichment functions and integration for crack modeling using the extended finite element method, J. Multiscale Comput. Eng. 11 (2013) 597–631.
[12] S. Nicaise, Y. Renard, E. Chahine, Optimal convergence analysis for the extended finite element method, Internat. J. Numer. Methods Engrg. 84 (2010) 1115–1138.
[13] E. Bechet, H. Minnebo, N. Moes, B. Burgardt, Improved implementation and robustness study of the X-FEM for stress analysis around cracks, Internat. J. Numer. Methods Engrg. 64 (2005) 1033–1056.
[14] A. Legay, H. Wang, T. Belytschko, Strong and weak arbitrary discontinuities in spectral finite elements, Internat. J. Numer. Methods Engrg. 64 (2005) 991–1008.
[15] K.W. Cheng, T.P. Fries, Higher-order XFEM for curved strong and weak discontinuities, Internat. J. Numer. Methods Engrg. 82 (2010) 564–590.
[16] K. Dreau, N. Chevaugeon, N. Moes, Studied X-FEM enrichment to handle material interfaces with higher order finite element, Comput. Methods Appl. Mech. Engrg. 199 (2010) 1922–1936.
[17] G. Legrain, N. Chevaugeon, K. Dreau, Studied X-FEM enrichment to handle material interfaces with higher order finite element, Comput. Methods Appl. Mech. Engrg. 241 (2012) 172–189.
[18] M. Moumnassi, S. Bellouettar, E. Bechet, S. Bordas, D. Quoirin, M. Potier-Ferry, Finite-element analysis on implicitly defined domains: an accurate representation based on arbitrary parametric surfaces, Comput. Methods Appl. Mech. Engrg. 200 (2011) 774–796.
[19] P.G. Ciarlet, The Finite Element Method for Elliptic Problems, North Holland, Amsterdam, 1979.
[20] G. Strang, G. Fix, An Analysis of the Finite Element Method, Prentice-Hall, Englewood cliffs, New Jersey, 1973.
[21] S. Osher, J.A. Sethian, Fronts propagations with curvature dependent speed: algorithms based on Hamilton–Jacobi formulations, J. Comput. Phys. 79 (1998) 12–49.
[22] J. Li, J.M. Melenk, B. Wohlmuth, J. Zou, Optimal a priori estimates for higher order finite elements for elliptic interface problems, Appl. Numer. Math. 60 (2010) 19–37.
[23] B. Flemisch, J. Melenk, B. Wohlmuth, Mortar methods with curved interfaces, Appl. Numer. Math. 54 (2005) 339–361.
[24] E.M. Stein, Singular Integrals and Differentiability Properties of Functions, Princeton University Press, Princeton, 1970.
[25] S. Amdouni, P. Hild, V. Lleras, M. Moakher, Y. Renard, A stabilized lagrange multiplier method for the enriched finite-element approximation of contact problems of cracked elastic bodies, Math. Modelling Numer. Anal. 49 (2012) 813–839.
[26] S. Amdouni, K. Mansouri, Y. Renard, M. Arfaoui, M. Moakher, Numerical convergence and stability of mixed formulation with X-FEM cutoff, Eur. J. Comput. Mech. 21 (2012) 160–173.
[27] N. Sukumar, D. Chopp, N. Moes, T. Belytschko, Modeling holes and inclusions by level-sets in the extended finite element method, Comput. Methods Appl. Mech. Engrg. 190 (2001) 6183–6200.